Mutual Information Maximization for SWIPT AF MIMO Relay Systems with Non-linear EH Models and Imperfect Channel State Information

Justin Bing Lee, *Student Member, IEEE*, Yue Rong, *Senior Member, IEEE*, Lenin Gopal, *Member, IEEE*, and Choo W. R. Chiong, *Member, IEEE*

Abstract—In this paper, we investigate a two-hop simultaneous wireless information and power transfer (SWIPT) amplify-and-forward (AF) multiple-input multiple-output (MIMO) relay communication system with an energy-limited relay node. The relay node harvests energy based on the radio-frequency (RF) signal transmitted from the source node through the time-switching (TS) protocol and fully uses the harvested energy to precode and forward the information to the destination node. The non-linear energy harvesting models are considered at the relay node. With the consideration of the channel estimation error, the joint optimization of the TS factor, source and relay precoding matrices is proposed with robustness against the channel state information (CSI) mismatch to maximize the mutual information (MI) between the source and destination nodes. The optimal structure for the source and relay precoding matrices is derived to simplify the transceiver optimization problem. Numerical simulations show that the system performance provided by the proposed algorithms with robustness is better than the non-robust algorithm.

Index Terms—Amplify-and-forward, energy harvesting, imperfect CSI, MIMO relay, robustness, simultaneous wireless information and power transfer (SWIPT), time-switching.

I. INTRODUCTION

Following the commercialization of the fifth-generation (5G) networks, the sixth-generation (6G) networks are visioned by researchers around the world to be developed into green networks [1]. Besides being eco-friendly wireless networks, 6G networks are also expected to provide an improved system capacity, data rate, and better quality of services. Hence, simultaneous wireless information and power transfer (SWIPT) technology plays a vital role in developing the 6G networks. The radio-frequency (RF) signals are utilized in the SWIPT technology by transferring information and power at the same time. In the early studies of the SWIPT technology

[2], an ideal receiver structure is proposed to perform information decoding (ID) and energy harvesting (EH) from the same received RF signals simultaneously. However, the ideal receiver is challenging to implement in practice [3]. This is because the practical EH circuits are unable to perform ID, and the practical ID circuits are unable to perform EH from the same received RF signals. Besides, wireless information transfer and wireless power transfer function in different sensitivity. In [4], two practical SWIPT receiver architectures are proposed, namely the time-switching (TS) receiver and the power-splitting (PS) receiver. In the TS receiver, a time-switch is installed at the receiving antenna to switch between the EH and ID circuits according to the designed TS-sequence. In the PS receiver, a PS unit is implemented at the receiving antenna to divide the received RF signals into two portions of signals, where one portion is used for ID whereas the remaining portion is used for EH. In [5], the problem of power minimization in SWIPT networks with coexisting PS and TS users has been studied under nonlinear EH model.

In the scenario where the source and destination nodes are located far apart, a relay node is needed to improve the system performance as it helps in extending the network coverage of wireless communication [6]. In [7], the authors extended the SWIPT receiver architectures by implementing them in the energy-constrained relay node, such EH relaying protocols are known as the TS relaying (TSR) protocol and the PS relaying (PSR) protocol [7]. The energy harvested by the SWIPT relay node is used to process and forward the received information signals to the destination node. In [8], the performance of a hybrid TSR and PSR protocol is analyzed with nonlinear energy harvester.

Generally, to improve the spectral and energy efficiency of a communication system, the multiple-input multiple-output (MIMO) technology is usually adopted. MIMO technology can be easily implemented by installing multiple antennas at the system nodes. Moreover, the MIMO technology also improves the efficiency for the RF energy transmission to wireless devices [9]. Recently, the application of SWIPT in MIMO relay systems with EH relay nodes has been studied in [9]–[13]. In [9], the authors investigate the system performance for a hybridized SWIPT MIMO relay system where the TSR and PSR are jointly implemented at the relay node to increase the energy harvested at the relay node. In [10], the source and relay precoding matrices are jointly optimized to achieve the maximal achievable rate for the amplify-and-forward (AF)

MIMO relay system with the relay node adopting either the TSR protocol or the PSR protocol. In [11], the optimization problem for a SWIPT MIMO relay communication system with the TSR protocol is investigated for an AF relay. In [12], the authors study the AF MIMO relay system with the relay node adopting the PSR protocol and tackle the joint optimization problem for the source and relay precoding matrices and the PS factor matrix by using several optimization techniques, such as the sequential quadratic programming approach and the semi-definite programming approach. In [13], the authors extend the investigation carried out in [11] and [12] to regenerative relays.

It can be noticed that in the existing studies [9]–[13], the channel state information (CSI) is assumed to be fully known at the receiving nodes. However, it is impossible to have the exact CSI in practice due to the channel estimation error. The mismatch between the estimated CSI and the exact CSI results in degradation of the system performance [14], [15]. In [16]–[20], the influence of the imperfect CSI in SWIPT MIMO relay systems is investigated. The authors of [16] and [17] study the impact of CSI mismatch towards the MIMO relay system with the ideal SWIPT relay protocol. It is observed that the imperfect CSI considered in [16] and [17] is a special case, where the authors assumed the row and column covariance matrices for the CSI mismatch matrices as scaled identity matrices, and the CSI mismatch is treated as noise. However, in practical scenarios, the assumption in [16] and [17] is not valid, as often there is correlation in the elements of the channel matrix.

In this paper, with the consideration of imperfect CSI, we propose a transceiver design for a two-hop AF MIMO relay communication system where the relay node adopts the TSR protocol to harvest energy and applies the precode-and-forward operation to process the information signal. In contrast to [16] and [17], we consider the general case and do not assume any special form for the row and column covariance matrices, and the CSI mismatch is modeled based on the Gaussian-Kronecker model. In [18], a SWIPT relay system is investigated with the consideration of CSI mismatch, where one antenna is chosen from the source node and the Jth best single-antenna relay node is selected. Transmit antenna selection strategy is used in [19] to reduce the system complexity for a dual-hop SWIPT MIMO AF relay communication system with consideration of the imperfect CSI. It is observed that the system nodes which transmit information, e.g., the source node and the relay node, are treated as single-antenna system nodes in [19]. Thus, the systems in [18] and [19] are essentially single-input single-output (SISO) systems, which can only transmit one data stream. Different to [18] and [19], all the antennas considered in this paper are used to transmit/receive RF signal, which enables multiple parallel data streams to be transmitted simultaneously. Note that the performance gain of a multi-antenna relay over a single-antenna relay node decreases with the increasing correlation among multiple antennas.

In [20], an energy-efficient design for a two-way MIMO relay network with the PSR protocol is investigated with the consideration of the CSI mismatch. Compared with [20], a one-way MIMO relay scenario (e.g. wireless broadcasting) is considered in this paper. Moreover, the PSR protocol requires high complexity hardware implementation. Instead of the PSR protocol, we consider the TSR protocol in the relay node to harvest energy from the RF signal transmitted by the source node. Furthermore, the CSI mismatch considered in [18] is modeled based on the Euclidean-norm bounded model. The robust transceiver design based on the Euclidean norm-bounded CSI mismatch is commonly known as the worst-case based design, which tends to be pessimistic compared with the probability based robust design in this paper.

In [21], the harvest-use and harvest-use-store models are investigated with full-duplex EH relay communication systems using the PS-based relaying protocol. In [22], the impact of co-channel interference (CCI) towards a wireless communication system using a SWIPT full-duplex relay with the PS-based relaying protocol is studied. In [23], the achievable rate of full-duplex relay communication systems is studied under the TS-based EH relay protocol. Compared with half-duplex relays, full-duplex relaying has higher CCI, which increases the system outage probability [22]. Therefore, the half-duplex mode is considered in this paper.

To the best of our knowledge, there is no existing work carried out for the SWIPT AF MIMO relay system with the consideration of practical imperfect CSI based on the Gaussian-Kronecker model and the non-linear EH models at the relay node. Hence, to fill in the gap, this research is performed. It is demonstrated through numerical simulations that the proposed scheme enhances the robustness of the SWIPT AF MIMO relay system against the CSI mismatch.

The novelties/contributions of this paper are listed as follows:

- In this paper, the transceiver design is proposed based on a two-hop AF MIMO relay system with the TSR protocol, where the practical imperfect CSI and non-linear EH models are considered. The proposed algorithm in this paper provides better robustness compared to the existing algorithms.
- Different to [9]–[13], [16], [17], [19], [20], the transceiver design in this paper is based on the practical non-linear EH models. In practice, it is noted that the assumption of a linear EH model is not valid. It is commonly known that the EH circuit does not function when the input power is below the EH circuit power sensitivity threshold, whereas a standard EH circuit is not capable of providing more harvested power when the EH circuit reaches saturation [24]. In this paper, we consider three different non-linear EH models when optimizing the transceiver design. Hence, the proposed algorithms in this paper is applicable to different non-linear EH models.
- As compared to [16], a more general CSI mismatch based on the Gaussian-Kronecker model is considered in optimizing the system performance for a two-hop AF MIMO relay system. We would like to mention that the scenario considered in [16] is viewed as a special case, where there is no correlation in the elements of the channel matrix. However, this assumption is not valid in practice. In the case where the row and column covariance matrices

are not identity matrices, the optimization problem is more complicated to solve. Besides, we would like to highlight that the optimization problem with imperfect CSI considered in [16] assumed that the transmission energy used at the relay node is constant. In this paper, we consider the scenario where the harvested energy at the relay node is fully utilized to forward the signal to the destination node.

- The highly complicated optimization problem is simplified by using several approximation and optimization techniques. Besides, the structure of the source and relay precoding matrices is used to reduce the complexity of the complicated joint transceiver design problem to an optimal power allocation problem.
- Numerical simulations are carried out to validate the system performance of the proposed algorithms. As illustrated by the simulations examples, the proposed algorithms provide better system performance compared to the existing algorithm proposed in [11] in practical channel matrices.

The rest of this paper is organized as follows. In Section II, the system model of a two-hop MIMO relay system with an EH relay node is introduced with the consideration of imperfect CSI. The relay node harvests energy through the TSR protocol, and the harvested energy is fully used for processing and transmitting the information signals. In Section III, the robust transceiver design is proposed by using optimization techniques such as the primal decomposition method, the Karush-Kuhn-Tucker (KKT) conditions, and the golden section search method. In subsection III-D, the practical peak power limits are introduced to the proposed optimization problem. In Section IV, numerical simulations are presented to illustrate the system performance of the proposed algorithm. The paper is conclude in Section V.
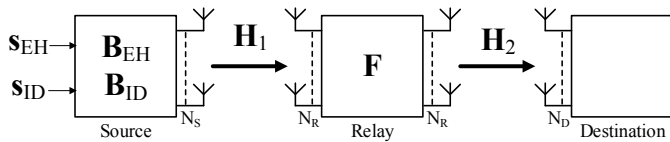
II. SYSTEM MODEL

Fig. 1. Block diagram of a two-hop MIMO relay system with an EH relay using the TS protocol.

In this paper, a two-hop three-node relay communication system as illustrated in Fig. 1 is considered, where the information signal is transmitted from the source node to the destination node through a relay node. The source, relay and destination nodes are respectively installed with N_S, N_R and N_D antennas. For the relay node, we select the AF relaying scheme due to its simplicity, where the received information-carrying signal is linearly precoded and forwarded to the destination node. The impact of the direct link between the source node and the destination node is assumed to be negligible due to severe shadowing and pathloss. The source node is equipped with an individual power supply where a given power budget of P_s is allocated for the source node

to transmit information signal. However, the relay node is an energy-limited wireless-powered device where it is required to be powered by the energy harvested from the received RF signals.
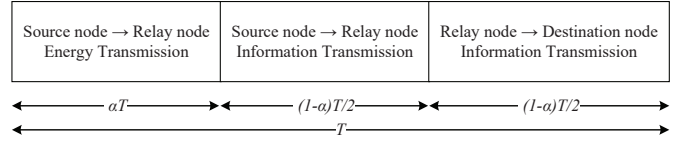

Fig. 2. The diagram of the TS protocol.

With the TS protocol implemented for EH at the relay node, a full communication cycle with the duration of T is separated into three sections as illustrated in Fig. 2. In the first time frame with a duration of αT, where $\alpha \in (0,1)$ is the TS factor, the source node precodes and transmits the signal vector $\mathbf{s}_e$ to the relay node with the source node precoding matrix at the first time frame denoted as $\mathbf{B}_e$, where $\mathbf{s}_e$ is the energy-bearing signal with covariance matrix given as $\mathrm{E}\{\mathbf{s}_e\mathbf{s}_e^H\} = \mathbf{I}_{N_e}$. Here, $\mathrm{E}\{\cdot\}$ denotes the statistical expectation, $(\cdot)^H$ denotes the Hermitian matrix transpose and $\mathbf{I}_m$ denotes a size m identity matrix. Hence, the received signal vector at the relay node for EH during the first time frame is given as

$$\mathbf{y}_{r,e} = \mathbf{H}_1\mathbf{B}_e\mathbf{s}_e + \mathbf{n}_{r,e} \qquad (1)$$

where $\mathbf{H}_1$ is the first hop MIMO channel matrix in the communication system, $\mathbf{n}_{r,e}$ is the additive white Gaussian noise (AWGN) introduced at the relay node during the first time frame. In this paper, the energy harvested at the relay node is modelled based on the non-linear EH models. For the non-linear EH model, the constant-linear-constant (CLC) EH model [24], the logistic function (LF) EH model [25] and the heuristic EH model [26] are considered in this paper. Hence, the energy harvested at the relay node is expressed as

$$\tilde{E}_r = \alpha E_h\left(tr\left\{\mathbf{H}_1\mathbf{B}_e\mathbf{B}_e^H\mathbf{H}_1^H\right\}\right) \qquad (2)$$

where $tr\{\cdot\}$ denotes the matrix trace and $E_h(x)$ represents the applied EH model and it is expressed as

$$E_h(x) = \begin{cases} E_{clc}(x) & \text{if CLC EH} \\ \dfrac{\frac{E'_m}{1+\exp(-a(x-b))} - E'_m \mathcal{Z}}{1 - \mathcal{Z}} & \text{if LF EH} \\ x\eta_h(x) & \text{if heuristic EH} \end{cases} \qquad (3)$$

where $E_{clc}(x)$ is a piecewise function as

$$E_{clc}(x) = \begin{cases} 0, & x \le P_{Th} \\ E'_m, & \eta x \ge E'_m \\ \eta x, & \text{otherwise} \end{cases} , \qquad (4)$$

$\eta \in (0,1)$ is the energy harvesting efficiency, P_{Th} and E'_m respectively denote the minimum input power and the maximum output power of a practical EH circuit, $\mathcal{Z} = (1 + \exp(ab))^{-1}$, $\exp(\cdot)$ represents the exponential function, a and b are experimental parameters related to the EH circuit specification such as impedance and diode forward voltage, $\eta_h(x)$ is given as

$$\eta_h(x) = \frac{c_0 + c_1 x + c_2 x^2}{d_0 + d_1 x + d_2 x^2 + d_3 x^3}, \qquad (5)$$

where the input power x to the function $\eta_h(\cdot)$ is in milliwatts and the output efficiency $\eta_h(\cdot)$ is in percentage, $c_0, c_1, c_2, d_0, d_1, d_2$ and d_3 are the parameters which depend on the EH circuits.

In the second time frame with a duration of $(1-\alpha)T/2$, the source node precodes and transmits the signal vector $\mathbf{s}_i$ to the relay node with the source node precoding matrix at the second time frame denoted as $\mathbf{B}_i$, where $\mathbf{s}_i$ is the information-carrying signal with the covariance matrix given as $\mathrm{E}\{\mathbf{s}_i\mathbf{s}_i^H\} = \mathbf{I}_{N_i}$ and $N_i = \min(N_S, N_R, N_D)$. The received signal vector at the relay node for ID during the second time frame is given as

$$\mathbf{y}_{r,i} = \mathbf{H}_1\mathbf{B}_i\mathbf{s}_i + \mathbf{n}_{r,i} \quad (6)$$

where $\mathbf{n}_{r,i}$ is the AWGN introduced at the relay node during the second time frame with the noise covariance matrix given as $\mathrm{E}\{\mathbf{n}_{r,i}\mathbf{n}_{r,i}^H\} = \sigma_r^2\mathbf{I}_{N_R}$.

During the final time frame with a duration of $(1-\alpha)T/2$, using the AF protocol, the relay node precodes and forwards the received signal vector $\mathbf{y}_{r,i}$ to the destination node with the relay node precoding matrix denoted as $\mathbf{F}$. The received signal at the destination node is given as

$$\mathbf{y}_d = \mathbf{H}_2\mathbf{F}\mathbf{H}_1\mathbf{B}_i\mathbf{s}_i + \mathbf{H}_2\mathbf{F}\mathbf{n}_{r,i} + \mathbf{n}_d \quad (7)$$

where $\mathbf{H}_2$ is the second hop MIMO channel matrix in the communication system and $\mathbf{n}_d$ is the AWGN introduced at the destination node with the noise covariance matrix given as $\mathrm{E}\{\mathbf{n}_d\mathbf{n}_d^H\} = \sigma_d^2\mathbf{I}_{N_D}$. For simplicity, we set $T = 1$. We assume that without wasting the available transmission power at the source and relay node, $\mathrm{r}(\mathbf{B}_i) = \mathrm{r}(\mathbf{F}) = N_i$, where $\mathrm{r}(\cdot)$ denotes the rank of a matrix.

Different from the ideal situation, the CSI is partially known at the relay and destination nodes in practice. This is because of the channel estimation error which results in the mismatch between the exact CSI and the estimated CSI. Hence, the true MIMO channel matrices with consideration of the CSI mismatch are given as

$$\mathbf{H}_1 = \widehat{\mathbf{H}}_1 + \mathbf{\Delta}_1, \quad \mathbf{H}_2 = \widehat{\mathbf{H}}_2 + \mathbf{\Delta}_2 \quad (8)$$

where $\widehat{\mathbf{H}}_1$ and $\widehat{\mathbf{H}}_2$ are the estimated channel matrices for the first and the second hop of the communication system, whereas $\mathbf{\Delta}_1$ and $\mathbf{\Delta}_2$ are the respective CSI mismatch matrices. Generally, $\mathbf{\Delta}_1$ can be equivalently expressed as $\mathbf{\Sigma}_1^{\frac{1}{2}}\mathbf{\Delta}_{\omega,1}\mathbf{\Phi}_1^{\frac{1}{2}}$ as shown in [27], [28], where $\mathbf{\Sigma}_1$ and $\mathbf{\Phi}_1$ respectively represent the row and column covariance matrices of $\mathbf{\Delta}_1$, whereas $\mathbf{\Delta}_{\omega,1}$ is an $N_S \times N_R$ complex Gaussian matrix with zero-mean and unit-variance independent and identically distributed (i.i.d.) entries. Similar to $\mathbf{\Delta}_1$, $\mathbf{\Delta}_2$ can be expressed as $\mathbf{\Sigma}_2^{\frac{1}{2}}\mathbf{\Delta}_{\omega,2}\mathbf{\Phi}_2^{\frac{1}{2}}$, where $\mathbf{\Sigma}_2$ and $\mathbf{\Phi}_2$ respectively represent the row and column covariance matrices of $\mathbf{\Delta}_2$, whereas $\mathbf{\Delta}_{\omega,2}$ is an $N_D \times N_R$ complex Gaussian matrix whose entries are i.i.d. with zero-mean and unit variance. Thus, $\mathbf{\Delta}_1$ and $\mathbf{\Delta}_2$ follow the Gaussian Kronecker model as

$$\mathbf{\Delta}_1 \sim \mathcal{CN}(\mathbf{0}, \mathbf{\Sigma}_1 \otimes \mathbf{\Phi}_1^T), \quad \mathbf{\Delta}_2 \sim \mathcal{CN}(\mathbf{0}, \mathbf{\Sigma}_2 \otimes \mathbf{\Phi}_2^T) \quad (9)$$

where $\otimes$ denotes the matrix Kronecker product. As highlighted in [27], the expressions of $\mathbf{\Sigma}_1, \mathbf{\Sigma}_2, \mathbf{\Phi}_1$ and $\mathbf{\Phi}_2$ generally

rely on the specific channel estimation algorithms. We would like to note that although the Gaussian-Kronecker model is a classical CSI mismatch model, the algorithms developed in this paper are applicable to other CSI mismatch distributions, as long as the mean and the covariance of the CSI mismatch matrices are given.

By substituting (8) into (7), the received signal at the destination node with the consideration of CSI mismatch can be equivalently rewritten as

$$\begin{aligned}
\mathbf{y}_d &= \widehat{\mathbf{H}}_2\mathbf{F}\widehat{\mathbf{H}}_1\mathbf{B}_i\mathbf{s}_i + \widehat{\mathbf{H}}_2\mathbf{F}\left(\mathbf{\Delta}_1\mathbf{B}_i\mathbf{s}_i + \mathbf{n}_{r,i}\right) \\
&\quad + \mathbf{\Delta}_2\mathbf{F}\left(\widehat{\mathbf{H}}_1\mathbf{B}_i\mathbf{s}_i + \mathbf{\Delta}_1\mathbf{B}_i\mathbf{s}_i + \mathbf{n}_{r,i}\right) + \mathbf{n}_d \\
&\triangleq \widehat{\mathbf{H}}\mathbf{s}_i + \mathbf{n}
\end{aligned} \quad (10)$$

where

$$\widehat{\mathbf{H}} \triangleq \widehat{\mathbf{H}}_2\mathbf{F}\widehat{\mathbf{H}}_1\mathbf{B}_i \quad (11)$$

$$\begin{aligned}
\mathbf{n} &\triangleq \widehat{\mathbf{H}}_2\mathbf{F}\left(\mathbf{\Delta}_1\mathbf{B}_i\mathbf{s}_i + \mathbf{n}_{r,i}\right) \\
&\quad + \mathbf{\Delta}_2\mathbf{F}\left(\widehat{\mathbf{H}}_1\mathbf{B}_i\mathbf{s}_i + \mathbf{\Delta}_1\mathbf{B}_i\mathbf{s}_i + \mathbf{n}_{r,i}\right) + \mathbf{n}_d.
\end{aligned} \quad (12)$$

Here, $\widehat{\mathbf{H}}$ can be viewed as the estimated MIMO channel matrix between the source node and the destination node, whereas $\mathbf{n}$ is the total noise introduced throughout the system due to noise at the receiving antennas and the channel estimation error. Meanwhile, the covariance matrix for $\mathbf{n}$ is expressed as

$$\mathbf{R}_n = \widehat{\mathbf{H}}_2\mathbf{F}\left(\gamma_1\mathbf{\Sigma}_1 + \sigma_r^2\mathbf{I}_{N_R}\right)\mathbf{F}^H\widehat{\mathbf{H}}_2^H + \gamma_2\mathbf{\Sigma}_2 + \sigma_d^2\mathbf{I}_{N_D} \quad (13)$$

where

$$\gamma_1 = tr\left\{\mathbf{B}_i\mathbf{B}_i^H\mathbf{\Phi}_1\right\}$$

$$\gamma_2 = tr\left\{\mathbf{F}\left(\widehat{\mathbf{H}}_1\mathbf{B}_i\mathbf{B}_i^H\widehat{\mathbf{H}}_1^H + \gamma_1\mathbf{\Sigma}_1 + \sigma_r^2\mathbf{I}_{N_R}\right)\mathbf{F}^H\mathbf{\Phi}_2\right\}.$$

When the CSI is fully known at the receiving nodes, the actual mutual information (MI), $\mathcal{I}_{SD}$ between the source and destination node [11] is given as

$$\begin{aligned}
\mathcal{I}_{SD} = \frac{1-\alpha}{2}\log_2\Big|\mathbf{I}_{N_i} &+ \mathbf{B}_i^H\mathbf{H}_1^H\mathbf{F}^H\mathbf{H}_2^H \\
&\times \left(\sigma_r^2\mathbf{H}_2\mathbf{F}\mathbf{F}^H\mathbf{H}_2^H + \sigma_d^2\mathbf{I}_{N_D}\right)^{-1}\mathbf{H}_2\mathbf{F}\mathbf{H}_1\mathbf{B}_i\Big| \quad (14)
\end{aligned}$$

where $|\cdot|$ and $(\cdot)^{-1}$ respectively denote the determinant and inverse of a matrix. However, the actual $\mathcal{I}_{SD}$ is unknown in practice due to the imperfect CSI [28]–[30]. Similar to [28]–[30], the lower-bound of the actual $\mathcal{I}_{SD}$ which is given as

$$\mathcal{I}_{SD}^{(low)} = \frac{1-\alpha}{2}\log_2\left|\mathbf{I}_{N_i} + \widehat{\mathbf{H}}^H\mathbf{R}_n^{-1}\widehat{\mathbf{H}}\right|, \quad (15)$$

is adopted in this paper. Furthermore, with the consideration of channel mismatch, it is noted that

$$\begin{aligned}
&\mathrm{E}_H\left\{tr\left\{\mathbf{H}_1\mathbf{B}_e\mathbf{B}_e^H\mathbf{H}_1^H\right\}\right\} \\
&= tr\left\{\widehat{\mathbf{H}}_1\mathbf{B}_e\mathbf{B}_e^H\widehat{\mathbf{H}}_1^H + tr\{\mathbf{B}_e\mathbf{B}_e^H\mathbf{\Phi}_1\}\mathbf{\Sigma}_1\right\} \\
&= tr\left\{\mathbf{B}_e\mathbf{B}_e^H\left(\widehat{\mathbf{H}}_1^H\widehat{\mathbf{H}}_1 + tr\{\mathbf{\Sigma}_1\}\mathbf{\Phi}_1\right)\right\} \quad (16)
\end{aligned}$$

where $\mathrm{E}_H\{\cdot\}$ denotes the statistical expectation with respect to $\mathbf{H}_1$ and $\mathbf{H}_2$.

The transmission energy required at the source node for the first time frame and the second time frame are respectively

given as $\alpha tr\{\mathbf{B}_e\mathbf{B}_e^H\}$ and $\frac{1-\alpha}{2}tr\{\mathbf{B}_i\mathbf{B}_i^H\}$, thus the transmission energy constraint at the source node is expressed as

$$\alpha tr\{\mathbf{B}_e\mathbf{B}_e^H\} + \frac{1-\alpha}{2}tr\{\mathbf{B}_i\mathbf{B}_i^H\} \leq \frac{1+\alpha}{2}P_s. \quad (17)$$

Moreover, the transmission energy needed at the relay node E_u is given as

$$E_u = \frac{1-\alpha}{2}tr\left\{\mathbf{F}\left(\widehat{\mathbf{H}}_1\mathbf{B}_i\mathbf{B}_i^H\widehat{\mathbf{H}}_1^H + \gamma_1\mathbf{\Sigma}_1 + \sigma_r^2\mathbf{I}_{N_R}\right)\mathbf{F}^H\right\}. \quad (18)$$

With the consideration that the relay node is an energy-constrained device, the available transmission energy at the relay node solely relies on the harvested energy. Hence, the transmission energy constraint at the relay node is given as

$$E_u \leq E_r \quad (19)$$

where $E_r = \alpha E_h\left(tr\left\{\mathbf{B}_e\mathbf{B}_e^H\mathbf{Q}\right\}\right)$. Here, $\mathbf{Q} = \widehat{\mathbf{H}}_1^H\widehat{\mathbf{H}}_1 + tr\{\mathbf{\Sigma}_1\}\mathbf{\Phi}_1$ is introduced with corresponding eigenvalue decomposition (EVD) given as $\mathbf{V}_q\mathbf{\Lambda}_q\mathbf{V}_q^H$, where $\mathbf{\Lambda}_q$ is a diagonal matrix with its diagonal elements sorted in descending order.

The objective of this paper is to obtain the optimal $\alpha, \mathbf{B}_e, \mathbf{B}_i$ and $\mathbf{F}$ to maximize $\mathcal{I}_{SD}^{(low)}$, subjecting to the transmission energy constraint at the source node and the relay node which are respectively given as (17) and (19). Hence, the optimization problem is expressed as

$$\max_{\alpha,\mathbf{B}_e,\mathbf{B}_i,\mathbf{F}} \frac{1-\alpha}{2}\log_2\left|\mathbf{I}_{N_i} + \widehat{\mathbf{H}}^H\mathbf{R}_n^{-1}\widehat{\mathbf{H}}\right| \quad (20a)$$

$$s.t. \ \alpha tr\{\mathbf{B}_e\mathbf{B}_e^H\} + \frac{1-\alpha}{2}tr\{\mathbf{B}_i\mathbf{B}_i^H\} \leq \frac{1+\alpha}{2}P_s \quad (20b)$$

$$E_u \leq E_r, \quad 0 < \alpha < 1. \quad (20c)$$

III. PROPOSED TRANSCEIVER OPTIMIZATION ALGORITHM

Theorem 1: The optimal $\mathbf{B}_e$ as the solution to the problem (20) has the following structure

$$\mathbf{B}_e^* = \lambda_e^{\frac{1}{2}}\mathbf{v}_{q,1}\mathbf{u}_1^H \quad (21)$$

where $(\cdot)^*$ denotes the optimal value, λ_e is a positive scalar variable, $\mathbf{v}_{q,1}$ denotes the first column of $\mathbf{V}_q$ and $\mathbf{u}_1$ is an $N_e \times 1$ vector satisfying $\mathbf{u}_1^H\mathbf{u}_1 = 1$.

Proof: Refer to Appendix A. ∎

Theorem 1 shows that the optimal $\mathbf{B}_e$ has a rank-one solution. It can be seen from (21) that the source node sends one energy beam towards the strongest direction $\mathbf{v}_{q,1}$ of the source-relay channel correlation matrix $\mathbf{Q}$, which is reasonable for the sake of energy transmission efficiency. With the optimal structure of $\mathbf{B}_e$ proposed in (21), the optimization problem (20) is rewritten as

$$\max_{\alpha,\lambda_e,\mathbf{B}_i,\mathbf{F}} \frac{1-\alpha}{2}\log_2\left|\mathbf{I}_{N_i} + \widehat{\mathbf{H}}^H\mathbf{R}_n^{-1}\widehat{\mathbf{H}}\right| \quad (22a)$$

$$s.t. \ \alpha\lambda_e + \frac{1-\alpha}{2}tr\{\mathbf{B}_i\mathbf{B}_i^H\} \leq \frac{1+\alpha}{2}P_s \quad (22b)$$

$$E_u \leq \alpha E_h\left(\lambda_e\lambda_q\right), \ \lambda_e \geq 0, \ 0 < \alpha < 1 \quad (22c)$$

where λ_q is the largest eigenvalue of $\mathbf{Q}$. It can be observed that in the optimization problem (22), we only need to optimize λ_e in $\mathbf{B}_e$, where $tr\left\{\mathbf{B}_e\mathbf{B}_e^H\right\} = \lambda_e$.

The transceiver optimization problem (22) is nonconvex with matrix variables, where both the complicated objective function (22a) and the constraints (22b) and (22c) are nonconvex. Therefore, the actual globally optimal solution of the problem (22) is intractable. To solve (22), we propose to use a tri-loop iterative algorithm which obtains a suboptimal solution with a tractable computational complexity. In this tri-loop algorithm, the outer loop is used to optimize α based on the golden section search. Built upon the primal decomposition approach, the middle loop provides the optimal structure of $\mathbf{F}$, while the inner loop finds the optimal power loading in $\mathbf{B}_i$ and $\mathbf{F}$. We would like to mention that to the best of our knowledge, it is not possible to compare the solution of the tri-loop iterative algorithm with the actual optimal solution of the problem (22), as the latter is unknown.

A. Outer Loop: Optimization of α

In the outer loop, the optimal α is obtained. It is observed that the objective function (22a) is a unimodal function of α and the feasibility region of the problem (22) specified by (22b) and (22c) monotonically increases with α. Hence, to obtain the optimal α, the golden section search method [31] is adopted. It is obvious that the optimization problem (22) with any given α can be re-expressed as

$$\min_{\lambda_e,\mathbf{B}_i,\mathbf{F}} \mathcal{I}\{\alpha\} = \log_2\left|\left(\mathbf{I}_{N_i} + \widehat{\mathbf{H}}^H\mathbf{R}_n^{-1}\widehat{\mathbf{H}}\right)^{-1}\right| \quad (23a)$$

$$s.t. \ \alpha\lambda_e + \frac{1-\alpha}{2}tr\{\mathbf{B}_i\mathbf{B}_i^H\} \leq \frac{1+\alpha}{2}P_s \quad (23b)$$

$$E_u \leq \alpha E_h\left(\lambda_e\lambda_q\right), \quad \lambda_e \geq 0, \quad (23c)$$

where $\mathcal{I}\{\alpha\}$ denotes the optimal value of (23a) with any given α. Equivalently, the objective function of (22a) can be rewritten as $\mathcal{H}\{\alpha\} = -\frac{1-\alpha}{2}\mathcal{I}\{\alpha\}$. We present the procedure of the golden section search method in Algorithm 1, where δ is the golden ratio ($\delta \approx 1.618$) and ε_1 is a small positive constant which is used to control the convergence of the loop.

Algorithm 1 Golden section search method to find the optimal α

Initialization: $\alpha_L = 0$ and $\alpha_U = 1$
1: **while** $|\alpha_U - \alpha_L| \geq \varepsilon_1$ **do**
2:      Set $a_1 = (\delta - 1)\alpha_L + (2 - \delta)\alpha_U$.
3:      Set $a_2 = (2 - \delta)\alpha_L + (\delta - 1)\alpha_U$.
4:      Compute $\mathcal{H}\{a_1\}$ and $\mathcal{H}\{a_2\}$.
5:      **if** $\mathcal{H}\{a_1\} \leq \mathcal{H}\{a_2\}$ **then**
6:          $\alpha_L = a_1$.
7:      **else**
8:          $\alpha_U = a_2$.
9:      **end if**
10: **end while**
11: $\alpha^* = (\alpha_L + \alpha_U)/2$.

B. Middle Loop: Primal Decomposition

Next, we will tackle the optimization problem (23). With the matrix inversion lemma and the introduction of the optimal structure of $\mathbf{F}$ [32] given as

$$\mathbf{F}^* = \mathbf{TD} \quad (24)$$

where $\mathbf{D} = \mathbf{B}_i^H \widehat{\mathbf{H}}_1^H \left(\widehat{\mathbf{H}}_1 \mathbf{B}_i \mathbf{B}_i^H \widehat{\mathbf{H}}_1^H + \gamma_1 \mathbf{\Sigma}_1 + \sigma_r^2 \mathbf{I}_{N_R} \right)^{-1}$ can be viewed as a weight matrix for the Wiener filter at the relay node, whereas $\mathbf{T}$ is an $N_R \times N_i$ matrix which can be viewed as the relay transmit precoding matrix, (23a) can be rewritten as

$$\mathcal{I}\{\alpha\} = \log_2 \left| \left(\mathbf{I}_{N_i} + \mathbf{B}_i^H \widehat{\mathbf{H}}_1^H \mathbf{\Xi}_1^{-1} \widehat{\mathbf{H}}_1 \mathbf{B}_i \right)^{-1} \right.$$
$$\left. + \left(\mathbf{\Theta}^{-1} + \mathbf{T}^H \widehat{\mathbf{H}}_2^H \mathbf{\Xi}_2^{-1} \widehat{\mathbf{H}}_2 \mathbf{T} \right)^{-1} \right| \quad (25)$$

where

$$\mathbf{\Xi}_1 = tr \left\{ \mathbf{B}_i \mathbf{B}_i^H \mathbf{\Phi}_1 \right\} \mathbf{\Sigma}_1 + \sigma_r^2 \mathbf{I}_{N_R} \quad (26)$$
$$\mathbf{\Xi}_2 = tr \left\{ \mathbf{T}\mathbf{\Theta}\mathbf{T}^H \mathbf{\Phi}_2 \right\} \mathbf{\Sigma}_2 + \sigma_d^2 \mathbf{I}_{N_D} \quad (27)$$
$$\mathbf{\Theta} = \mathbf{B}_i^H \widehat{\mathbf{H}}_1^H \left(\widehat{\mathbf{H}}_1 \mathbf{B}_i \mathbf{B}_i^H \widehat{\mathbf{H}}_1^H + \mathbf{\Xi}_1 \right)^{-1} \widehat{\mathbf{H}}_1 \mathbf{B}_i. \quad (28)$$

By using (24), E_u is expressed as

$$E_u = \frac{1-\alpha}{2} tr \left\{ \mathbf{T}\mathbf{\Theta}\mathbf{T}^H \right\}. \quad (29)$$

Hence, the optimization problem (23) is rewritten as

$$\min_{\lambda_e, \mathbf{B}_i, \mathbf{T}} \log_2 \left| \left(\mathbf{I}_{N_i} + \mathbf{B}_i^H \widehat{\mathbf{H}}_1^H \mathbf{\Xi}_1^{-1} \widehat{\mathbf{H}}_1 \mathbf{B}_i \right)^{-1} \right. \quad (30a)$$
$$\left. + \left(\mathbf{\Theta}^{-1} + \mathbf{T}^H \widehat{\mathbf{H}}_2^H \mathbf{\Xi}_2^{-1} \widehat{\mathbf{H}}_2 \mathbf{T} \right)^{-1} \right|$$
$$s.t. \ \alpha\lambda_e + \frac{1-\alpha}{2} tr\{\mathbf{B}_i \mathbf{B}_i^H\} \leq \frac{1+\alpha}{2} P_s \quad (30b)$$
$$\frac{1-\alpha}{2} tr \left\{ \mathbf{T}\mathbf{\Theta}\mathbf{T}^H \right\} \leq \alpha E_h \left(\lambda_e \lambda_q \right) \quad (30c)$$
$$\lambda_e \geq 0. \quad (30d)$$

It is observed that in the problem (30), the optimal λ_e, $\mathbf{B}_i$ and $\mathbf{T}$ are coupled together, where the optimal λ_e is connected to the optimal $\mathbf{B}_i$ and $\mathbf{T}$ in the constraint (30b) and (30c) respectively, whereas $\mathbf{B}_i$ and $\mathbf{T}$ are linked together through the optimal λ_e. Hence, the primal decomposition method [33] is applied with the introduction of κ where $\alpha\lambda_e = \kappa$ and $\kappa \in [0, \frac{1+\alpha}{2} P_s]$. The master problem is written as

$$\min_{\kappa} \ \mathcal{I}\{\alpha\}(\kappa) = \log_2 \left| \left(\mathbf{I}_{N_i} + \mathbf{B}_i^H \widehat{\mathbf{H}}_1^H \mathbf{\Xi}_1^{-1} \widehat{\mathbf{H}}_1 \mathbf{B}_i \right)^{-1} \right.$$
$$\left. + \left(\mathbf{\Theta}^{-1} + \mathbf{T}^H \widehat{\mathbf{H}}_2^H \mathbf{\Xi}_2^{-1} \widehat{\mathbf{H}}_2 \mathbf{T} \right)^{-1} \right| \quad (31a)$$
$$s.t. \ 0 \leq \kappa \leq \frac{1+\alpha}{2} P_s \quad (31b)$$

where $\mathcal{I}\{\alpha\}(\kappa)$ denotes the optimal value of (31a) with any given κ. The optimization subproblem is given as

$$\min_{\mathbf{B}_i, \mathbf{T}} \log_2 \left| \left(\mathbf{I}_{N_i} + \mathbf{B}_i^H \widehat{\mathbf{H}}_1^H \mathbf{\Xi}_1^{-1} \widehat{\mathbf{H}}_1 \mathbf{B}_i \right)^{-1} \right.$$
$$\left. + \left(\mathbf{\Theta}^{-1} + \mathbf{T}^H \widehat{\mathbf{H}}_2^H \mathbf{\Xi}_2^{-1} \widehat{\mathbf{H}}_2 \mathbf{T} \right)^{-1} \right| \quad (32a)$$
$$s.t. \ tr\{\mathbf{B}_i \mathbf{B}_i^H\} \leq P_\alpha \quad (32b)$$
$$tr \left\{ \mathbf{T}\mathbf{\Theta}\mathbf{T}^H \right\} \leq E_\alpha \quad (32c)$$

where

$$P_\alpha = \frac{(1+\alpha)P_s - 2\kappa}{1-\alpha}, \quad E_\alpha = \frac{2\alpha}{1-\alpha} E_h \left(\frac{\kappa}{\alpha} \lambda_q \right). \quad (33)$$

In the middle loop, the master problem is solved by using a one-dimensional search method to obtain the optimal κ. For the one-dimensional search method, we use the well-known golden section search method [31]. The algorithm in solving the problem (31) is presented in Algorithm 2, where n is the number of iterations and ε_2 is a small positive number controlling the convergence of the algorithm.

Algorithm 2 Obtain the optimal λ_e^* by solving the master problem (31)

    Initialization: $n = 0$, $\kappa_{lo}^{\{0\}} = 0$ and $\kappa_{up}^{\{0\}} = \frac{1+\alpha}{2} P_s$
1: **while** $|\kappa_{up}^{\{n\}} - \kappa_{lo}^{\{n\}}| \geq \varepsilon_2 \kappa_{up}^{\{0\}}$ **do**
2:      Set $k_1^{\{n\}} = (\delta - 1)\kappa_{lo}^{\{n\}} + (2 - \delta)\kappa_{up}^{\{n\}}$.
3:      Set $k_2^{\{n\}} = (2 - \delta)\kappa_{lo}^{\{n\}} + (\delta - 1)\kappa_{up}^{\{n\}}$.
4:      Compute $\mathcal{I}\{\alpha\}(k_1^{\{n\}})$ and $\mathcal{I}\{\alpha\}(k_2^{\{n\}})$.
5:      **if** $\mathcal{I}\{\alpha\}(k_1^{\{n\}}) \geq \mathcal{I}\{\alpha\}(k_2^{\{n\}})$ **then**
6:          $\kappa_{lo}^{\{n+1\}} = k_1^{\{n\}}$, $\kappa_{up}^{\{n+1\}} = \kappa_{up}^{\{n\}}$.
7:      **else**
8:          $\kappa_{lo}^{\{n+1\}} = \kappa_{lo}^{\{n\}}$, $\kappa_{up}^{\{n+1\}} = k_2^{\{n\}}$.
9:      **end if**
10:      $n = n + 1$.
11: **end while**
12: $\kappa^* = (\kappa_{lo}^{\{n\}} + \kappa_{up}^{\{n\}})/2$.
13: $\lambda_e^* = \kappa^*/\alpha$.

C. Inner Loop: Optimization of $\mathbf{B}_i$ and $\mathbf{T}$

In the innermost loop, we solve the problem (32). By using the matrix inversion lemma, it is noted that $\mathbf{\Theta}$ can be rewritten as

$$\mathbf{\Theta} = \mathbf{B}_i^H \widehat{\mathbf{H}}_1^H \mathbf{\Xi}_1^{-1} \widehat{\mathbf{H}}_1 \mathbf{B}_i \left(\mathbf{B}_i^H \widehat{\mathbf{H}}_1^H \mathbf{\Xi}_1^{-1} \widehat{\mathbf{H}}_1 \mathbf{B}_i + \mathbf{I}_{N_i} \right)^{-1} (34)$$

whereas it is noticed that at moderately high SNRs, i.e. $\mathbf{B}_i^H \widehat{\mathbf{H}}_1^H \mathbf{\Xi}_1^{-1} \widehat{\mathbf{H}}_1 \mathbf{B}_i \gg \mathbf{I}_{N_i}$, $\mathbf{\Theta} \approx \mathbf{I}_{N_i}$. Hence, at moderately high SNRs, $\mathbf{\Xi}_2$ is given as

$$\mathbf{\Xi}_2 = tr \left\{ \mathbf{T}\mathbf{T}^H \mathbf{\Phi}_2 \right\} \mathbf{\Sigma}_2 + \sigma_d^2 \mathbf{I}_{N_D} \quad (35)$$

and the problem (32) is expressed as

$$\min_{\mathbf{B}_i, \mathbf{T}} \log_2 \left| \left(\mathbf{I}_{N_i} + \mathbf{B}_i^H \widehat{\mathbf{H}}_1^H \mathbf{\Xi}_1^{-1} \widehat{\mathbf{H}}_1 \mathbf{B}_i \right)^{-1} \right.$$
$$\left. + \left(\mathbf{I}_{N_i} + \mathbf{T}^H \widehat{\mathbf{H}}_2^H \mathbf{\Xi}_2^{-1} \widehat{\mathbf{H}}_2 \mathbf{T} \right)^{-1} \right| \quad (36a)$$
$$s.t. \ tr\{\mathbf{B}_i \mathbf{B}_i^H\} \leq P_\alpha \quad (36b)$$
$$tr \left\{ \mathbf{T}\mathbf{T}^H \right\} \leq E_\alpha. \quad (36c)$$

Furthermore, we would like to mention that in general scenarios, the CSI mismatch covariance matrices, $\mathbf{\Phi}_1, \mathbf{\Phi}_2, \mathbf{\Sigma}_1$ and $\mathbf{\Sigma}_2$ are not scaled identity matrices as assumed in [16]. This is because in many practical applications, there is channel correlation [27]. Thus, it is more difficult to solve the problem (36) as compared to [16]. To reduce the difficulties in solving the problem (36), the following inequality is used [27]

$$tr \left\{ \mathbf{X}\mathbf{Y} \right\} \leq tr \left\{ \mathbf{X} \right\} \lambda_M(\mathbf{Y}) \quad (37)$$

where $\lambda_M(\cdot)$ denotes the largest eigenvalue of a matrix with equality holds when $\mathbf{Y}$ is a scaled identity matrix. By applying (37), the upper-bounds of $\boldsymbol{\Xi}_1$ and $\boldsymbol{\Xi}_2$ are respectively given as

$$\hat{\boldsymbol{\Xi}}_1[tr\{\mathbf{B}_i\mathbf{B}_i^H\}] = \phi_{1,1}tr\left\{\mathbf{B}_i\mathbf{B}_i^H\right\}\boldsymbol{\Sigma}_1 + \sigma_r^2\mathbf{I}_{N_R} \quad (38)$$

$$\hat{\boldsymbol{\Xi}}_2[tr\{\mathbf{T}\mathbf{T}^H\}] = \phi_{2,1}tr\left\{\mathbf{T}\mathbf{T}^H\right\}\boldsymbol{\Sigma}_2 + \sigma_d^2\mathbf{I}_{N_D} \quad (39)$$

with dependence on $tr\{\mathbf{B}_i\mathbf{B}_i^H\}$ and $tr\{\mathbf{T}\mathbf{T}^H\}$ where $\phi_{1,1} = \lambda_M(\boldsymbol{\Phi}_1)$ and $\phi_{2,1} = \lambda_M(\boldsymbol{\Phi}_2)$. Besides, it is clear that the equality of (36b) and (36c) must be satisfied with the optimal $\mathbf{B}_i$ and $\mathbf{T}$. Hence, the upper-bounds of $\boldsymbol{\Xi}_1$ and $\boldsymbol{\Xi}_2$ with the optimal $\mathbf{B}_i$ and $\mathbf{T}$ are expressed as

$$\hat{\boldsymbol{\Xi}}_1[P_\alpha] = \phi_{1,1}P_\alpha\boldsymbol{\Sigma}_1 + \sigma_r^2\mathbf{I}_{N_R}, \quad \hat{\boldsymbol{\Xi}}_2[E_\alpha] = \phi_{2,1}E_\alpha\boldsymbol{\Sigma}_2 + \sigma_d^2\mathbf{I}_{N_D}. \quad (40)$$

To reduce the complexity of the optimization problem (36), we replace $\boldsymbol{\Xi}_1$ and $\boldsymbol{\Xi}_2$ in (36a) with the corresponding upper-bounds. By exploiting the upper-bound of the objective function (32a), the optimization subproblem is transformed into

$$\min_{\mathbf{B}_i,\mathbf{T}} \log_2\left|\left(\mathbf{I}_{N_i} + \mathbf{B}_i^H\mathbf{M}\mathbf{B}_i\right)^{-1} + \left(\mathbf{I}_{N_i} + \mathbf{T}^H\mathbf{N}\mathbf{T}\right)^{-1}\right| \quad (41a)$$

$$s.t.\ tr\{\mathbf{B}_i\mathbf{B}_i^H\} \le P_\alpha \quad (41b)$$

$$tr\left\{\mathbf{T}\mathbf{T}^H\right\} \le E_\alpha \quad (41c)$$

where $\mathbf{M} = \hat{\mathbf{H}}_1^H(\hat{\boldsymbol{\Xi}}_1[P_\alpha])^{-1}\hat{\mathbf{H}}_1$ and $\mathbf{N} = \hat{\mathbf{H}}_2^H(\hat{\boldsymbol{\Xi}}_2[E_\alpha])^{-1}\hat{\mathbf{H}}_2$ with the corresponding EVD given as $\mathbf{V}_m\boldsymbol{\Lambda}_m\mathbf{V}_m^H$ and $\mathbf{V}_n\boldsymbol{\Lambda}_n\mathbf{V}_n^H$, where $\boldsymbol{\Lambda}_m$ and $\boldsymbol{\Lambda}_n$ are diagonal matrices with their diagonal elements arranged in descending order.

We would like to note that the purpose of applying the bounds in (35) and (37) is to make the problem (32) solvable with a practical computational complexity. Since the objective function (32a) is a complicated nonconvex function of matrix variables $\mathbf{B}_i$ and $\mathbf{T}$, the globally optimal solution of the problem (32) is intractable. Thus, it is very difficult to infer the gap between the global optimum of the problem (32) and the optimal solution of the problem (41).

Based on the Hadamard's inequality [34], for a positive semidefinite (PSD) matrix $\mathbf{X}$ of order N, the determinant of $\mathbf{X}$ follows the inequality introduced as

$$|\mathbf{X}| \le \prod_{i=1}^{N} x_i \quad (42)$$

where x_i denotes the ith diagonal element of $\mathbf{X}$. The equality of (42) is achieved when $\mathbf{X}$ is a diagonal matrix. Based on (42), the objective function (41a) is optimized when $\mathbf{B}_i^H\mathbf{M}\mathbf{B}_i$ and $\mathbf{T}^H\mathbf{N}\mathbf{T}$ are diagonal matrices. Hence, to optimize the objective function (41a), the optimal structure for $\mathbf{B}_i$ and $\mathbf{T}$ is given as

$$\mathbf{B}_i^* = \mathbf{V}_{m,1}\boldsymbol{\Lambda}_b^{\frac{1}{2}}\ ,\ \mathbf{T}^* = \mathbf{V}_{n,1}\boldsymbol{\Lambda}_t^{\frac{1}{2}} \quad (43)$$

where $\boldsymbol{\Lambda}_b$ and $\boldsymbol{\Lambda}_t$ are diagonal matrices with non-negative entries, whereas $\mathbf{V}_{m,1}$ and $\mathbf{V}_{n,1}$ contain the leftmost N_i columns of $\mathbf{V}_m$ and $\mathbf{V}_n$ respectively.

By substituting (43) into (41), the problem (41) is equivalently reduced to a power allocation problem with scalar variables which is given as

$$\min_{\boldsymbol{\lambda}_b,\boldsymbol{\lambda}_t} \sum_{i=1}^{N_i} \log_2\left(\frac{1}{1+\lambda_{m,i}\lambda_{b,i}} + \frac{1}{1+\lambda_{n,i}\lambda_{t,i}}\right) \quad (44a)$$

$$s.t. \sum_{i=1}^{N_i} \lambda_{b,i} \le P_\alpha \quad (44b)$$

$$\sum_{i=1}^{N_i} \lambda_{t,i} \le E_\alpha \quad (44c)$$

$$\lambda_{b,i} \ge 0\ ,\ \lambda_{t,i} \ge 0\ ,\ i = 1,\cdots,N_i \quad (44d)$$

where $\boldsymbol{\lambda}_b = [\lambda_{b,1},\cdots,\lambda_{b,N_i}]^T$, $\boldsymbol{\lambda}_t = [\lambda_{t,1},\cdots,\lambda_{t,N_i}]^T$ and for $i = 1,\cdots,N_i$, $\lambda_{m,i}$, $\lambda_{n,i}$, $\lambda_{b,i}$ and $\lambda_{t,i}$ denote the ith diagonal element of $\boldsymbol{\Lambda}_m$, $\boldsymbol{\Lambda}_n$, $\boldsymbol{\Lambda}_b$ and $\boldsymbol{\Lambda}_t$, respectively. It is observed that the objective function (44a) is symmetric in $\boldsymbol{\lambda}_b$ and $\boldsymbol{\lambda}_t$, whereas the optimal $\boldsymbol{\lambda}_b$ and $\boldsymbol{\lambda}_t$ have different transmission power constraint. Hence, we propose a bi-step iterative method [35]–[37] to solve the problem (44), in which the optimal $\boldsymbol{\lambda}_b$ and $\boldsymbol{\lambda}_t$ are iteratively updated until convergence. Firstly, we solve the problem (44) with fixed $\boldsymbol{\lambda}_t$. By using the Lagrange multiplier method, it is noted that the optimal $\lambda_{b,i}^*$ for $i = 1,\cdots,N_i$ to the problem (44) with any given $\boldsymbol{\lambda}_t$ is given as

$$\lambda_{b,i}^* = \frac{1}{2\lambda_{m,i}}\left(\sqrt{z_i^2 + \frac{4\lambda_{m,i}z_i}{\mu_1}} - z_i - 2\right)^+ \quad (45)$$

where $z_i = 1 + \lambda_{n,i}\lambda_{t,i}$ for $i = 1,\cdots,N_i$, $(x)^+ = \max(0,x)$, and $\mu_1 > 0$ is the Lagrangian multiplier to (44b) and can be calculated by solving the equality of (44b) with $\lambda_{b,i}^*$ given in (45) using the bisection method.

Similarly, the optimal $\lambda_{t,i}^*$ for $i = 1,\cdots,N_i$ to the problem (44) with any given $\boldsymbol{\lambda}_b$ is given as

$$\lambda_{t,i}^* = \frac{1}{2\lambda_{n,i}}\left(\sqrt{y_i^2 + \frac{4\lambda_{n,i}y_i}{\mu_2}} - y_i - 2\right)^+ \quad (46)$$

where $y_i = 1 + \lambda_{m,i}\lambda_{b,i}$ for $i = 1,\cdots,N_i$, $\mu_2 > 0$ is the Lagrangian multiplier to (44c) and can be calculated by solving the equality of (44c) with $\lambda_{t,i}^*$ given in (46) using the bisection method. The bi-step iterative algorithm in solving the power allocation problem (44) is summarized in Algorithm 3, where ε_3 is a small positive number controlling the convergence of the algorithm.

The main complexity of solving the problem (22) using the proposed tri-loop algorithm is in calculating the EVD of $\mathbf{M}$ and $\mathbf{N}$ in (41), which has a complexity order of $\mathcal{O}(N_S^3)$ and $\mathcal{O}(N_R^3)$, respectively. Thus, the overall computational complexity of the tri-loop algorithm is given by $\mathcal{O}(c_1c_2(N_S^3 + N_R^3))$, where c_1 is the number of golden section searches in Algorithm 1 to obtain the optimal α, and c_2 is the number of iterations in solving the master problem (31) in Algorithm 2.

Algorithm 3 Bi-step iterative algorithm to solve the problem (44)

Initialization: $\lambda_{b,i}^{\{0\}} = \frac{P_\alpha}{N_i}$ and $\lambda_{t,i}^{\{0\}} = \frac{E_\alpha}{N_i}$, $\forall i$

1: $n = 0$, flag = 1.
2: **while** flag = 1 **do**
3: $\quad n \leftarrow n + 1$.
4: $\quad$ Calculate $\lambda_{b,i}^*, \forall i$ with fixed $\boldsymbol{\lambda}_t^{\{n-1\}}$ and set it as $\boldsymbol{\lambda}_b^{\{n\}}$.
5: $\quad$ Calculate $\lambda_{t,i}^*, \forall i$ with fixed $\boldsymbol{\lambda}_b^{\{n\}}$ and set it as $\boldsymbol{\lambda}_t^{\{n\}}$.
6: $\quad$ **if** $\max |\boldsymbol{\lambda}_b^{\{n\}} - \boldsymbol{\lambda}_b^{\{n-1\}}| \le \varepsilon_3$ **then**
7: $\qquad$ **if** $\max |\boldsymbol{\lambda}_t^{\{n\}} - \boldsymbol{\lambda}_t^{\{n-1\}}| \le \varepsilon_3$ **then**
8: $\qquad\quad$ flag = 0, $m = n$.
9: $\qquad$ **end if**
10: $\quad$ **end if**
11: **end while**
12: $\boldsymbol{\lambda}_b^* = \boldsymbol{\lambda}_b^{\{m\}}$ and $\boldsymbol{\lambda}_t^* = \boldsymbol{\lambda}_t^{\{m\}}$.

D. Peak Power Constraints

We would like to highlight the fact that under the transmission energy constraint at the source node (17), when α approaches its boundary [4], i.e., $\alpha \to 0$ and $\alpha \to 1$, the transmission powers for the source node, i.e., $tr\{\mathbf{B}_e \mathbf{B}_e^H\}$ and $tr\{\mathbf{B}_i \mathbf{B}_i^H\}$ may approach infinity, which is not achievable in practice. Moreover, when $\alpha \to 1$, from (19), the relay node transmission power may approach infinity. Thus, to impose the practical peak power constraints to the optimization problem (30), we introduce $\hat{P}_s$ and $\hat{P}_r$ as the peak power limits at the source node and the relay node respectively, with the corresponding peak transmission power constraints given as $\lambda_e \le \hat{P}_s$, $tr\{\mathbf{B}_i \mathbf{B}_i^H\} \le \hat{P}_s$ and $tr\{\mathbf{T}\boldsymbol{\Theta}\mathbf{T}^H\} \le \hat{P}_r$. With the introduction of peak power limits, the optimization master problem (31) is rewritten as

$$\min_\kappa \ \mathcal{E}\{\alpha\}(\kappa) \tag{47a}$$

$$s.t. \ 0 \le \kappa \le \min\left(\frac{1+\alpha}{2}P_s, \alpha\hat{P}_s\right) \tag{47b}$$

whereas the optimization subproblem (32) is rewritten as

$$\min_{\mathbf{B}_i,\mathbf{T}} \log_2 \left| \left(\mathbf{I}_{N_i} + \mathbf{B}_i^H \widehat{\mathbf{H}}_1^H \boldsymbol{\Xi}_1^{-1} \widehat{\mathbf{H}}_1 \mathbf{B}_i\right)^{-1} \right.$$
$$\left. + \left(\boldsymbol{\Theta}^{-1} + \mathbf{T}^H \widehat{\mathbf{H}}_2^H \boldsymbol{\Xi}_2^{-1} \widehat{\mathbf{H}}_2 \mathbf{T}\right)^{-1} \right| \tag{48a}$$

$$s.t. \ tr\{\mathbf{B}_i \mathbf{B}_i^H\} \le \rho_s \tag{48b}$$

$$tr\{\mathbf{T}\boldsymbol{\Theta}\mathbf{T}^H\} \le \rho_r \tag{48c}$$

where $\rho_s = \min(P_\alpha, \hat{P}_s)$ and $\rho_r = \min(E_\alpha, \hat{P}_r)$.

By observation, it is noticed that the structure of the master problem (31) and the problem (47) is identical. Hence, Algorithm 2 can be used to solve the problem (47) with some modifications at the initialization step, i.e. instead of $\kappa_{up}^{\{0\}} = \frac{1+\alpha}{2}P_s$, $\kappa_{up}^{\{0\}}$ is initialized as $\kappa_{up}^{\{0\}} = \min\left(\frac{1+\alpha}{2}P_s, \alpha\hat{P}_s\right)$. Besides, it is also observed that structure for the optimization subproblem with peak power limits (48) is identical to the problem (32). Thus, the technique used in solving the problem (32) is adopted to solve the problem (48). Similar to the algorithm proposed to solve the problem (32), we have $\boldsymbol{\Theta} \approx \mathbf{I}_{N_i}$.

The upper-bound of $\boldsymbol{\Xi}_1$ and $\boldsymbol{\Xi}_2$ with the introduction of peak power limits is rewritten as

$$\hat{\boldsymbol{\Xi}}_1[\rho_s] = \phi_{1,1}\rho_s\boldsymbol{\Sigma}_1 + \sigma_r^2 \mathbf{I}_{N_R}, \quad \hat{\boldsymbol{\Xi}}_2[\rho_r] = \phi_{2,1}\rho_r\boldsymbol{\Sigma}_2 + \sigma_d^2 \mathbf{I}_{N_D}. \tag{49}$$

The problem (48) with the upper-bound of (48a) as objective function is expressed as

$$\min_{\mathbf{B}_i,\mathbf{T}} \log_2 \left| \left(\mathbf{I}_{N_i} + \mathbf{B}_i^H \mathbf{M}' \mathbf{B}_i\right)^{-1} + \left(\mathbf{I}_{N_i} + \mathbf{T}^H \mathbf{N}' \mathbf{T}\right)^{-1} \right| \tag{50a}$$

$$s.t. \ tr\{\mathbf{B}_i \mathbf{B}_i^H\} \le \rho_s \tag{50b}$$

$$tr\{\mathbf{T}\mathbf{T}^H\} \le \rho_r \tag{50c}$$

where $\mathbf{M}' = \widehat{\mathbf{H}}_1^H (\hat{\boldsymbol{\Xi}}_1[\rho_s])^{-1} \widehat{\mathbf{H}}_1$ and $\mathbf{N}' = \widehat{\mathbf{H}}_2^H (\hat{\boldsymbol{\Xi}}_2[\rho_r])^{-1} \widehat{\mathbf{H}}_2$ with corresponding EVDs given as $\mathbf{V}'_m \boldsymbol{\Lambda}'_m \mathbf{V}'^H_m$ and $\mathbf{V}'_n \boldsymbol{\Lambda}'_n \mathbf{V}'^H_n$ where $\boldsymbol{\Lambda}'_m$ and $\boldsymbol{\Lambda}'_n$ are diagonal matrices with their diagonal elements arranged in descending order.

Similar to (35), the bounds in (49) are used to make the problem (48) solvable with a practical computational complexity. It is hard to quantify the gap between the globally optimal solution of the problem (48) and the proposed solution via solving the problem (50), as the former is intractable to obtain. By using the optimal structure of $\mathbf{B}_i = \mathbf{V}'_m \boldsymbol{\Lambda}_b^{\frac{1}{2}}$ and $\mathbf{T} = \mathbf{V}'_n \boldsymbol{\Lambda}_t^{\frac{1}{2}}$, the problem (50) is expressed as

$$\min_{\boldsymbol{\lambda}_b,\boldsymbol{\lambda}_t} \sum_{i=1}^{N_i} \log_2\left(\frac{1}{1+\lambda'_{m,i}\lambda_{b,i}} + \frac{1}{1+\lambda'_{n,i}\lambda_{t,i}}\right) \tag{51a}$$

$$s.t. \ \sum_{i=1}^{N_i} \lambda_{b,i} \le \rho_s \tag{51b}$$

$$\sum_{i=1}^{N_i} \lambda_{t,i} \le \rho_r \tag{51c}$$

$$\lambda_{b,i} \ge 0, \ \lambda_{t,i} \ge 0, \ i = 1, \cdots, N_i \tag{51d}$$

where for $i = 1, \cdots, N_i$, $\lambda'_{m,i}$ and $\lambda'_{n,i}$ denote the ith diagonal elements of $\boldsymbol{\Lambda}'_m$ and $\boldsymbol{\Lambda}'_n$ respectively.

Similar to the method in solving the problem (44), the bi-step iterative algorithm presented in Algorithm 3 is used to solve the problem (51). With the consideration of peak power limits, the optimal $\lambda_{b,i}^*$ and $\lambda_{t,i}^*$ are proposed as follows. By using the Lagrange multiplier method, it is noted that the optimal $\lambda_{b,i}^*$ for $i = 1, \cdots, N_i$ to the problem (51) with any given $\boldsymbol{\lambda}_t$ is written as

$$\lambda_{b,i}^* = \frac{1}{2\lambda'_{m,i}} \left(\sqrt{z_i'^2 + \frac{4\lambda'_{m,i}z_i'}{\mu_1'}} - z_i' - 2\right)^+ \tag{52}$$

where $z_i' = 1 + \lambda'_{n,i}\lambda_{t,i}$ for $i = 1, \cdots, N_i$, and $\mu_1' > 0$ is the Lagrangian multiplier to (51b) and can be calculated by solving the equality of (51b) with $\lambda_{b,i}^*$ given in (52) using the bisection method. Similarly, the optimal $\lambda_{t,i}^*$ for $i = 1, \cdots, N_i$ to the problem (51) with any given $\boldsymbol{\lambda}_b$ is given as

$$\lambda_{t,i}^* = \frac{1}{2\lambda'_{n,i}} \left(\sqrt{y_i'^2 + \frac{4\lambda'_{n,i}y_i'}{\mu_2'}} - y_i' - 2\right)^+ \tag{53}$$

where $y'_i = 1 + \lambda'_{m,i}\lambda_{b,i}$ for $i = 1, \cdots, N_i$, $\mu'_2 > 0$ is the Lagrangian multiplier to (51c) and can be calculated by solving the equality of (51c) with $\lambda^*_{t,i}$ given in (53) using the bisection method.

Similar to the analysis before, the complexity of the transceiver optimization with peak power constraints using the tri-loop algorithm is $\mathcal{O}(c'_1 c'_2 (N_S^3 + N_R^3))$, where c'_1 is the number of golden section searches to obtain the optimal α, and c'_2 is the number of iterations in solving the master problem (47).

IV. NUMERICAL SIMULATIONS
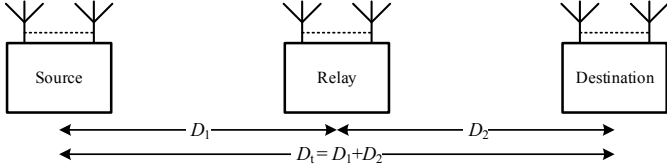
Fig. 3. Location of the source, relay, and destination nodes in the relay communication system.

In this section, we investigate the system performance of the proposed robust transceiver designs without peak power limits (Flexible) and with peak power limits (Peak). The transceiver design for the Flexible system is obtained by the proposed tri-loop algorithm where the problem (44) (i.e., the design criterion is (44a)) is solved in the inner loop. The MI of the Flexible system shown in the simulation figures is calculated according to (15) with α^* from Algorithm 1, $\mathbf{B}_i$ in (43) using $\mathbf{\Lambda}_b$ from Algorithm 3, and $\mathbf{F}^*$ in (24) with $\mathbf{T}^*$ in (43) using $\mathbf{\Lambda}_t$ from Algorithm 3. For the Peak system, the transceiver design is obtained using the tri-loop algorithm, where the problem (51) is solved in the inner loop, i.e., the design criterion is (51a). In the simulation figures, the MI of the Peak system is computed based on (15) in a way similar to the MI of the Flexible system described above, except that $\mathbf{\Lambda}_b$ and $\mathbf{\Lambda}_t$ are obtained from solving the problem (51).

We assume the peak power limits are given as $\widehat{P}_s = \widehat{P}_r = gP_s$, $(g \geq 1)$. The nodes in the relay communication system are placed as illustrated in Fig. 3, where the distance between the source and relay nodes D_1 is set as $D_1 = 10\tau$ meters and the distance between the relay and destination nodes D_2 is set as $D_2 = 10(2 - \tau)$ meters. The distance between the source and the destination nodes, i.e., the total distance, is set as $D_t = 20$ meters. The value of τ, $(0 < \tau < 2)$, is normalized over a distance of 10 meters, so the relay position can be easily determined, i.e., when $D_1 < D_2$, the relay is placed closer to the source node, whereas $D_2 < D_1$ indicates the relay node is placed closer to the destination node. In the simulations, we set $0.1 \leq \tau \leq 1.9$, thus $D_1 \geq 1$ meters and $D_2 \geq 1$ meters.

With the consideration of channel pathloss, the channel matrices $\mathbf{H}_1$ and $\mathbf{H}_2$ are correspondingly modelled as $\mathbf{H}_1 = D_1^{-\xi/2} \left(\widehat{\mathbf{H}}_1 + \mathbf{\Delta}_1 \right)$ and $\mathbf{H}_2 = D_2^{-\xi/2} \left(\widehat{\mathbf{H}}_2 + \mathbf{\Delta}_2 \right)$, where $D_1^{-\xi/2}$ and $D_2^{-\xi/2}$ denote the large scale pathloss of the source-relay link and the relay-destination link, respectively, ξ

denotes the pathloss exponent with $\xi = 3$ (suburban communication case) [38]. Based on the Gaussian-Kronecker model, the estimated channel matrices $\widehat{\mathbf{H}}_1$ and $\widehat{\mathbf{H}}_2$ are constructed as

$$\widehat{\mathbf{H}}_1 = \sqrt{\frac{1-\sigma_e^2}{\sigma_e^2}} \mathbf{\Sigma}_1^{\frac{1}{2}} \widehat{\mathbf{H}}_{\omega,1} \mathbf{\Phi}_1^{\frac{1}{2}}, \quad \widehat{\mathbf{H}}_2 = \sqrt{\frac{1-\sigma_e^2}{\sigma_e^2}} \mathbf{\Sigma}_2^{\frac{1}{2}} \widehat{\mathbf{H}}_{\omega,2} \mathbf{\Phi}_2^{\frac{1}{2}} \tag{54}$$

where σ_e^2 stands for the variance of estimation error, whereas $\widehat{\mathbf{H}}_{\omega,1}$ and $\widehat{\mathbf{H}}_{\omega,2}$ denote the small-scale channel fading. Here, $\widehat{\mathbf{H}}_{\omega,1}$ and $\widehat{\mathbf{H}}_{\omega,2}$ are complex Gaussian matrices whose entries are i.i.d. with zero mean and variance of $1/N_S$ and $1/N_R$ respectively.

The row and column covariance matrices for $\widehat{\mathbf{H}}_1, \widehat{\mathbf{H}}_2, \mathbf{\Delta}_1$ and $\mathbf{\Delta}_2$ are simulated as

$$[\mathbf{\Phi}_1]_{ij} = \sigma_e^2 \beta_t^{|i-j|} \quad i,j = 1, \cdots, N_S$$
$$[\mathbf{\Sigma}_1]_{ij} = \beta_r^{|i-j|} \quad i,j = 1, \cdots, N_R$$
$$[\mathbf{\Phi}_2]_{ij} = \sigma_e^2 \beta_t^{|i-j|} \quad i,j = 1, \cdots, N_R$$
$$[\mathbf{\Sigma}_2]_{ij} = \beta_r^{|i-j|} \quad i,j = 1, \cdots, N_D$$

where $[\cdot]_{ij}$ stands for the ith row jth column matrix entry, $\beta_t \in [0,1]$ and $\beta_r \in [0,1]$ denote the correlation coefficients of the row and column covariance matrices.

The parameters for all numerical examples are set as follows unless explicitly mentioned: where $N_S = N_R = N_D = N$, $\sigma_r^2 = \sigma_d^2 = -50$ dBm, $\varepsilon_1 = \varepsilon_2 = \varepsilon_3 = 10^{-6}$, $g = 2$, $\tau = 1$, $\sigma_e^2 = 0.1$, $\beta_t = 0.2$ and $\beta_r = 0.2$. The obtained simulation results are averaged through 500 independent channel realizations.

A. System performance comparison for the proposed robust algorithms and the existing non-robust algorithm given in [11].

In the first numerical example, the system performance for the proposed robust transceiver designs without peak power limits (Flexible) and with peak power limits (Peak) is compared to the upper-bound based algorithm developed in [11] using the estimated CSI (denoted as "Non-Robust"). The upper-bound based algorithm developed in [11] using the perfect CSI (denoted as "Perfect CSI") is set as the benchmark in the simulation and it is used to illustrate the system performance in the ideal scenario where there is no CSI mismatch. We would like to highlight that the Perfect CSI algorithm is not achievable in practice. In the existing work [11], it is noted that the linear EH model is used. Linear EH model can be viewed as a special case of the CLC non-linear EH model (denoted as "Ideal") where $P_{Th} = 0$ and $E'_m = \infty$. The practical CLC-EH model (denoted as "Practical") is mathematically formulated with $P_{Th} = -22.6$dBm and $E'_{max} = 20$mW [39]. For fairness, $\eta = 0.6$ is adopted for all the tested algorithms and $N = 3$. We compare the system MI for the tested algorithms at $\sigma_e^2 = 0.05$ and $\sigma_e^2 = 0.1$.

Fig. 4 and Fig. 5 correspondingly illustrate the system MI and the harvested energy at the relay node for all the tested systems at $\sigma_e^2 = 0.05$ and $\sigma_e^2 = 0.1$. Based on Fig. 4, it is observed that the proposed algorithms outperform the non-robust algorithm. Moreover, the system MI gap between
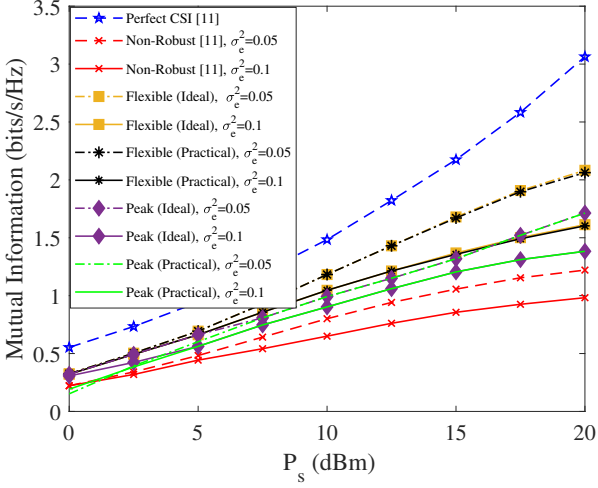
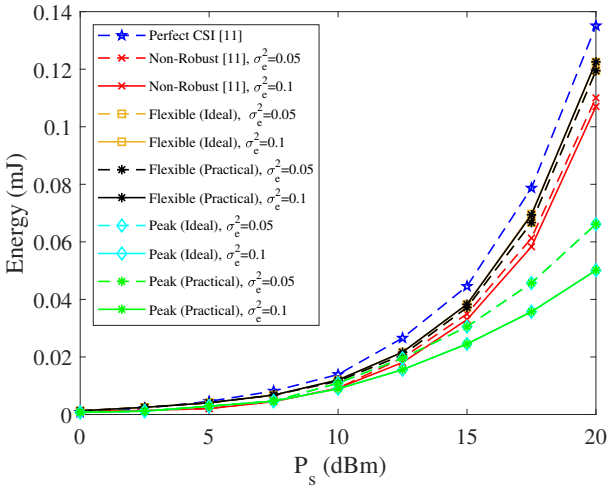Fig. 4. System MI for the tested algorithms versus P_s at $\sigma_e^2 = 0.05$ and $\sigma_e^2 = 0.1$.

Fig. 5. Harvested energy at the relay node for the tested algorithms versus P_s at $\sigma_e^2 = 0.05$ and $\sigma_e^2 = 0.1$.

the proposed robust algorithms and the non-robust algorithm is larger when σ_e^2 is greater. This observation indicates that the algorithm proposed without the consideration of the CSI mismatch will cause degradation in system performance in real life. Besides, it is noted from Fig. 5 that the energy harvested at the relay node for the non-robust algorithms is lower than the proposed algorithm. Furthermore, the system MI for the proposed algorithms with "Ideal" EH model and "Practical" EH model is almost identical at reasonably large P_s. This indicates that the practical EH circuit is not saturated with the energy-bearing signal transmitted to the relay node. Moreover, it is noted from the Fig. 4 that at low P_s (e.g. $P_s < 5$dBm), the system MI for the proposed algorithm with peak power limit using the "Practical" EH model is lower than the proposed algorithm with peak power limit using the "Ideal" EH mode. This is because the input power for the practical EH circuit with peak power limit in some circumstance is lower than the

EH circuit input power threshold (-22.6dBm), which results in zero transmission energy at the relay node. When the relay node does not have any transmission energy, the system MI is zero which results in low system MI as compared to the "Ideal" EH model algorithm.

B. System performance of the proposed robust algorithms with different non-linear EH model versus τ.
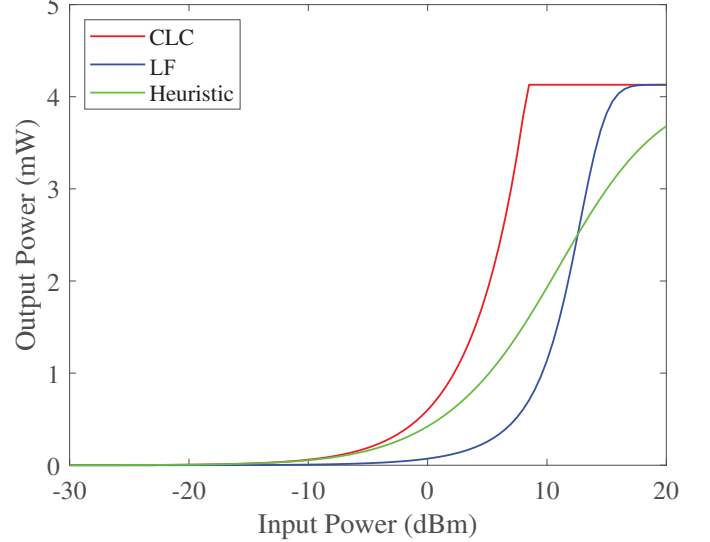
Fig. 6. The non-linear EH models for the EH circuit [47].
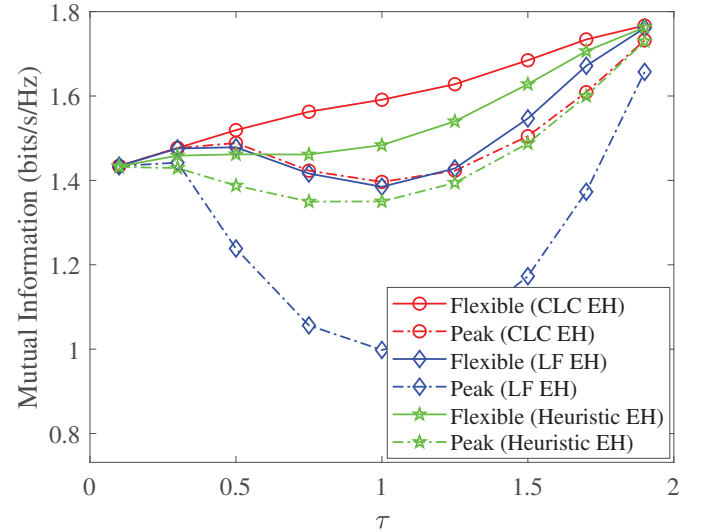
Fig. 7. System MI for the proposed algorithms against τ with the EH circuit [39] at $P_s = 20$dBm and $N = 2$.

In the second numerical example, we investigate the system performance for the proposed algorithm against τ at $P_s = 20$dBm and $N = 3$ with different non-linear EH models. For the CLC EH model, we set $P_{Th} = -22.6$dBm, $E'_m = 4$mW and $\eta = 0.6$. Similar to the CLC EH mode, the saturation output power for the LF EH model is set as 4mW, while the the experimental parameters are given as $a = 150$, $b = 0.014$ [40] (according to [42]). For the heuristic model
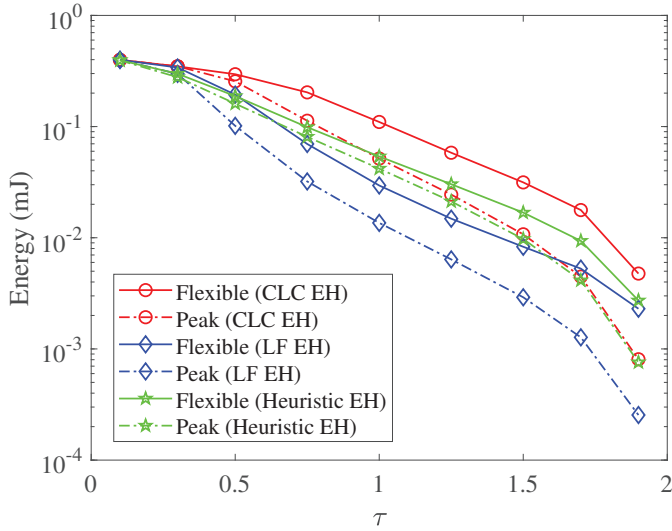
Fig. 8. Available energy at the relay node for the proposed algorithms against τ with the EH circuit [47] at $P_s = 20$dBm and $N = 2$.

[26], the experimental parameters are given as $c_0 = 704, c_1 = 1160, c_2 = 413, d_0 = 12.5, d_1 = 25.4, d_2 = 15.1$, and $d_3 = 1$ [47]. Fig. 6 illustrates the input-output energy relationship for the CLC EH model, the LF EH model and the heuristic EH model.

The CLC EH model considers the sensitivity and saturation output power with a constant energy harvesting efficiency at the linear range. The drawback of this non-linear EH model is that the saturation output power is not provided in many practical EH circuits e.g. [39]–[41], [44], [45]. Besides, the variation of the energy harvesting efficiency with respect to the input power is not reflected in this model. The merit of this model is in its simplicity. The LF EH model is constructed based on the logistic function (sigmoidal) to find the best-fit curves for the experimental data (output power) obtained from the EH circuit. The drawback of this model is that there is not much existing research with regards to EH circuits which includes the output power performance. Similar to the CLC EH mode, the saturation output power is commonly unknown. Moreover, in most cases, the experimental value b (which is used to represent the sensitivity) is different from the sensitivity value given by the EH circuit, e.g. for the circuit in [39] with $P_{Th} = 0.0055$mW, the curve fitting result in [25] shows $b = 0.003$. The benefit of this model is that it represents the practical rising edge of an EH circuit. Different to the LF EH model, the heuristic EH model is constructed based on the heuristic function to find the best-fit curve for the experimental data (energy efficiency) obtained from the EH circuit. The drawback of this model is there is not much work considering this non-linear EH model, hence not many experimental parameters can be obtained besides the work [26]. In addition, this EH model does not consider the sensitivity. It is noted that even though the input power is less than the sensitivity provided by the EH circuit, there is still output power. The benefit of this model is that it provides practical saturation output power and rising edge for EH circuits.

Fig. 7 and Fig. 8 correspondingly illustrate the system MI and the available energy at the relay node for the proposed algorithms against τ with different non-linear EH models. It can be observed from Fig. 8, the harvested energy for the proposed algorithms using the LF EH model is the lowest, whereas the harvested energy for the proposed algorithms using the CLC EH model is the highest. This agree with the input-output power relationship of the non-linear EH model used as illustrated in Fig. 6. Due to the difference in the harvested energy, it can be observed from Fig. 7 that the system MI for the proposed algorithms are different. It is observed that the system MI for the proposed algorithms increases when the relay node is placed further from the source node ($0.1 \leq \tau \leq 0.3$). By placing the relay node closer to the source node, it does not increase the available transmission energy at the relay node due to saturation of the EH circuit. For the heuristic model, it remains almost the same in this range. This is because the available transmission energy at the relay node is reduced with τ. However, when the relay node is located closer to the destination node, the system MI increased. This is because with a shorter distance between the relay and destination nodes which helps to improve the second-hop channel.

C. System MI for the proposed robust algorithms using the CLC EH model versus τ at different E'_m and P_{Th}.
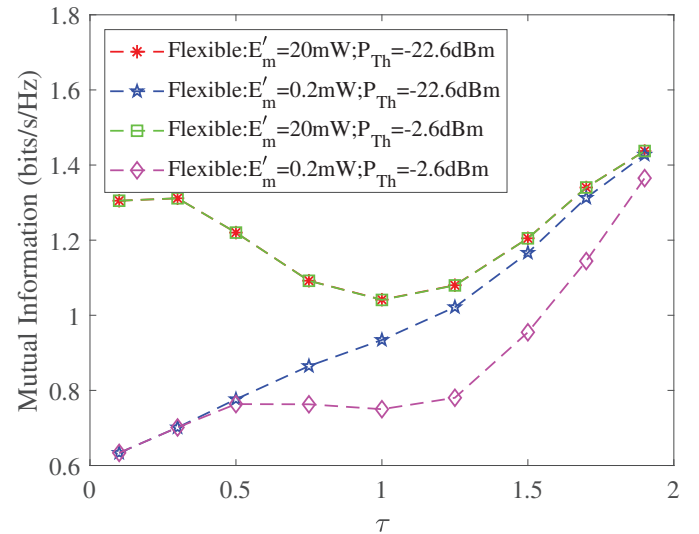

Fig. 9. System MI for the proposed algorithm without peak power limits using the CLC EH model versus τ with different E'_m and P_{Th} at $P_s = 15$dBm and $N = 2$.

In the third numerical example, we investigate the system MI for the proposed algorithm using the CLC EH model versus τ with different E'_m and P_{Th} at $P_s = 15$dBm and $N = 2$, where $E'_m = 20$mW or $E'_m = 0.2$mW whereas $P_{Th} = -22.6$dBm or $P_{Th} = -2.6$dBm. Fig. 9 illustrates the system MI for the proposed algorithm without peak power limits using the CLC EH model versus τ with various combinations of E'_m and P_{Th}. It is observed that the system MI for the proposed algorithm without peak power limits at $E'_m = 20$mW are identical. It is also noticed that there is a gap

in between the system MI for the proposed algorithm without peak power limits at $E'_m = 0.2$mW with different P_{Th}. The observation shows that the variation of P_{Th} does not impact the system MI for the proposed algorithm without peak power limits when the difference in P_{Th} and E'_m is sufficiently large. Furthermore, it is noticed that the system MI for the proposed algorithm without peak power limits at high E'_m decreased when the relay node is located further from the source node ($0.1 \leq \tau \leq 1$). This is because when the relay node is located further from the source node, the available transmission energy at the relay node which relies on the harvested energy reduces with τ. Interestingly, the system MI for the proposed algorithm without peak power limits at high E'_m increases when the relay node is located closer to the destination node. Even though at $1 \leq \tau \leq 1.9$, the available transmission energy at the relay node is reduced with τ, the distance between the relay node and the destination node is also reduced with τ. Due to the shorter distance between the relay and destination nodes, which leads to a better second-hop channel, the system MI increases. Unlike the system MI for the proposed algorithm without peak power limits at high E'_m, it is noticed that the system MI for the proposed algorithm without peak power limits at low E'_m increases with the increase of τ. This is because by placing the relay node closer to the source node does not help to increase the available transmission energy at the relay node as the output energy for the EH circuit at the relay is saturated. However, by placing the relay node closer to the destination node helps in providing better second-hop channel, hence the system MI increases with τ for the proposed algorithm with low E'_m.
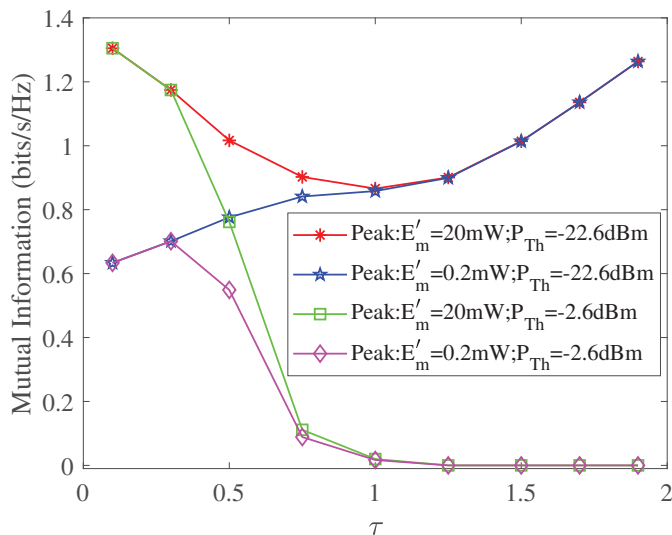

Fig. 10. System MI for the proposed algorithm with peak power limits using the CLC EH model versus τ with different E'_m and P_{Th} at $P_s = 15$dBm and $N = 2$.

Fig. 10 and Fig. 11 respectively illustrate the system MI and the available energy at the relay node for the proposed algorithm with peak power limits, $\hat{P}_s = \hat{P}_r = 2P_s$, using the CLC EH model versus τ with various combinations of E'_m and P_{Th}. It is observed that for the system MI of the proposed algorithms with peak power limits at low P_{Th}
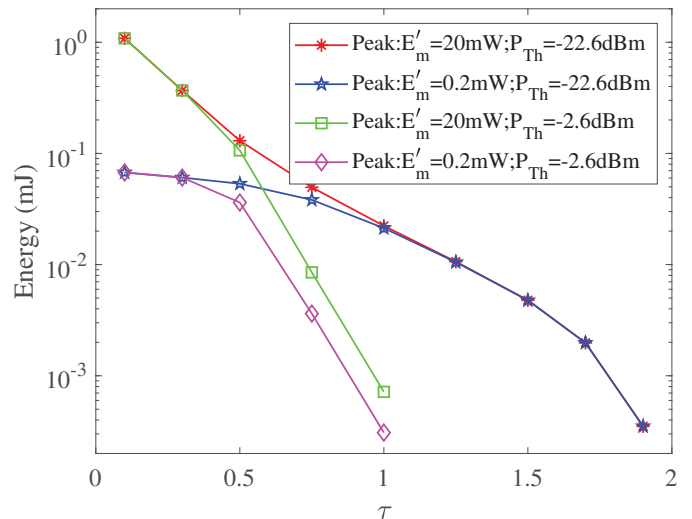

Fig. 11. Energy at the relay node for the proposed algorithm with peak power limit using the CLC EH model versus τ with different E'_m and P_{Th} at $P_s = 15$dBm and $N = 2$.

($P_{Th} = -22.6$dBm) follows a similar pattern as the system MI for the proposed algorithm without peak power limits as illustrated in Fig. 9. However, the system MI for the proposed algorithm with peak power limits at large P_{Th} ($P_{Th} = -2.6$dBm) is different to the system MI illustrated in Fig. 9. It is observed that the system MI for the proposed algorithm with peak power limits at large P_{Th} reduced to zero when $\tau > 1$. Besides, it is also noticed from Fig. 11, there is no transmission energy available at the relay node for the proposed system with $P_{Th} = -2.6$dBm when $\tau > 1$. This is because when the relay node is located further from the source node, the received RF signals for EH is reduced due to the channel pathloss and resulted in the received input power for the EH circuits below -2.6dBm. Different to the proposed algorithm without peak power limits, λ_e is capped by $\hat{P}_s$. As the source node is unable to provide sufficient transmission power (capped at $\hat{P}_s$) during the first time frame to activate the EH circuit, the system MI in practice is limited by the sensitivity of the EH circuit implemented at the relay node.

D. System MI for the proposed robust algorithms with peak power limits using the LF EH model versus τ with the EH circuit [40] and [41] at various E'_m.

In the fourth numerical example, we investigate the system MI for the proposed algorithm with peak power limits at $P_s = 15$dBm and $N = 3$ using the LF EH model against τ with the EH circuits proposed in [40] ($a = 150, b = 14$mW [42]) and [41] ($a = 47083, b = 2.9\mu$W [43]) at $E'_m = 20$mW and $E'_m = 10$mW. The LF EH model for the practical EH circuit at $E'_m = 20$mW and $E'_m = 10$mW is illustrated in Fig. 12. Based on Fig. 12, it is observed that the sensitivity for the EH circuit [40] is larger than the EH circuit [41]. Furthermore, it is also noticed that when a and b are fixed, the EH circuit using the LF EH model reaches the saturation output power at the same input power disregard the difference in the value of E'_m.
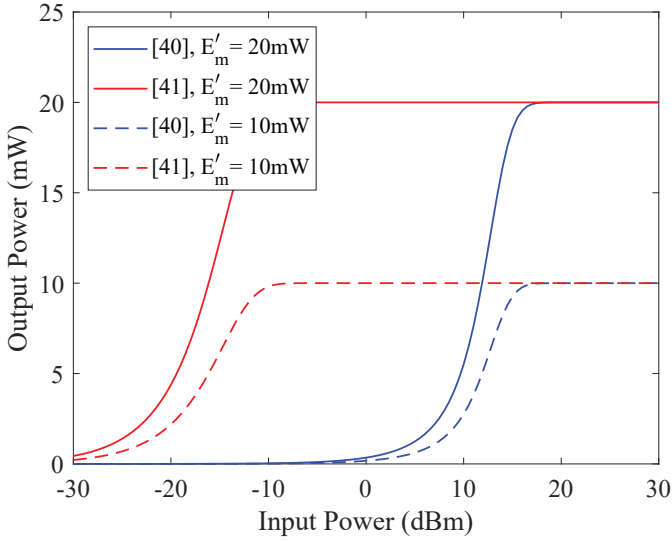
Fig. 12. The LF EH model representation of the EH circuits [40] and [41] at $E'_m = 20$mW and $E'_m = 10$mW.

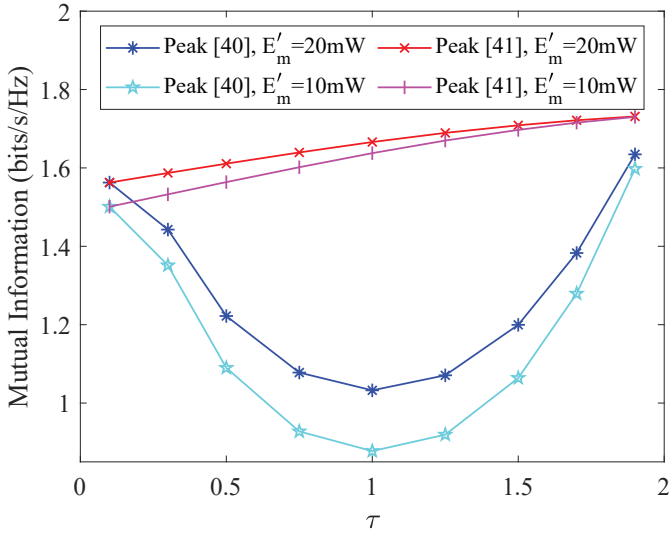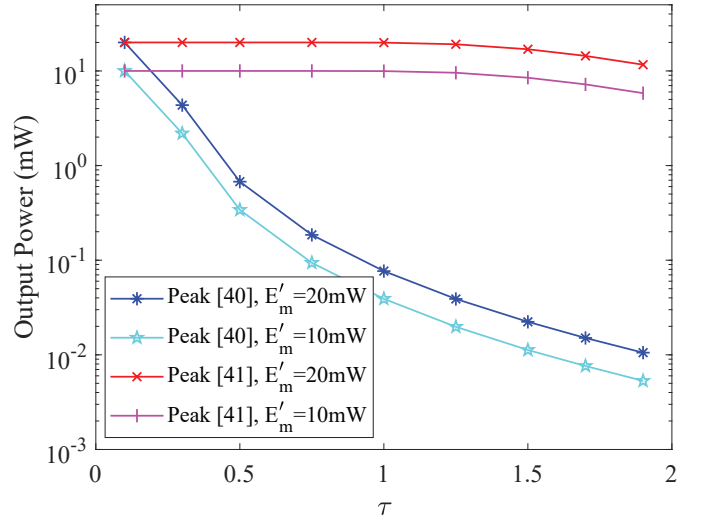Fig. 14. Output Energy of the EH circuit at the relay node for the proposed algorithm with peak power limits using the LF EH model versus τ at $P_s = 15$dBm, $N = 3$, with different E'_m ($E'_m = 20$mW and $E'_m = 10$mW) and the EH circuits [40] and [41].

Fig. 13. System MI for the proposed algorithm with peak power limits using the LF EH model versus τ at $P_s = 15$dBm, $N = 3$, with different E'_m ($E'_m = 20$mW and $E'_m = 10$mW) and the EH circuits [40] and [41].

Fig. 13 and Fig. 14 correspondingly illustrate the system MI and the output energy of the EH circuit at the relay node for the proposed algorithm with peak power limits at $P_s = 15$dBm, $N = 3$, with different E'_m ($E'_m = 20$mW and $E'_m = 10$mW) and the EH circuits [40] and [41]. At $0.1 \leq \tau \leq 1$, it is observed that the system MI for the proposed algorithm with the EH circuit [40] decreases when the relay node is located further from the source node. However, at $1 \leq \tau \leq 1.9$, the system MI for the proposed algorithm with the EH circuit [40] increases when the relay node is located nearer to the destination node. This is because by placing the relay node closer to the source node improves the amount of energy harvested at the relay node, whereas by placing the relay node closer to the destination node ensures better second-hop channel which helps to improve the system MI. It is observed from Fig. 14, the EH circuit [40] reaches its

saturation point when the relay node is located close to the source node. When the relay node is located further from the source node, the output energy significantly reduces. This is because by locating the relay node further from the source node, the received RF signals are significantly influenced by the channel pathloss which reduces the amount of input power to the EH circuit at the relay node. Thus, when the relay node is located further from the source node, the amount of energy harvested at the relay node is reduced. Furthermore, it is noticed that the system MI for the proposed algorithm with the EH circuit [41] is different to the system performance of the proposed algorithm with the EH circuit [40]. The system MI for the proposed algorithm with the EH circuit [41] increases when the relay node is located nearer to the destination node. Besides, it can be noticed from Fig. 14, the output power from the EH circuit [41] is not significantly decreased as compared to the EH circuit [40] when the relay node is located further from the source node. This is because the EH circuit [41] reaches the saturation output power at relatively low input power as shown in Fig. 12.

E. System MI for the proposed robust algorithms with peak power limits at $P_s = 20$dBm using the heuristic EH model versus τ with different practical EH circuit experimental parameters.

In the fifth numerical example, we investigate the system MI for the proposed algorithm with peak power limits at $P_s = 20$dBm and $N = 2$ using the heuristic EH model against τ with practical EH circuits proposed in [39], [41], [44], and [45]. The experimental parameters for the considered EH circuits are obtained based on the experimental parameters provided in [26].

Fig. 15 and Fig. 16 illustrate the system MI and the available energy at the relay node for the proposed algorithm with peak power limits using the heuristic EH model versus τ at $P_s =$
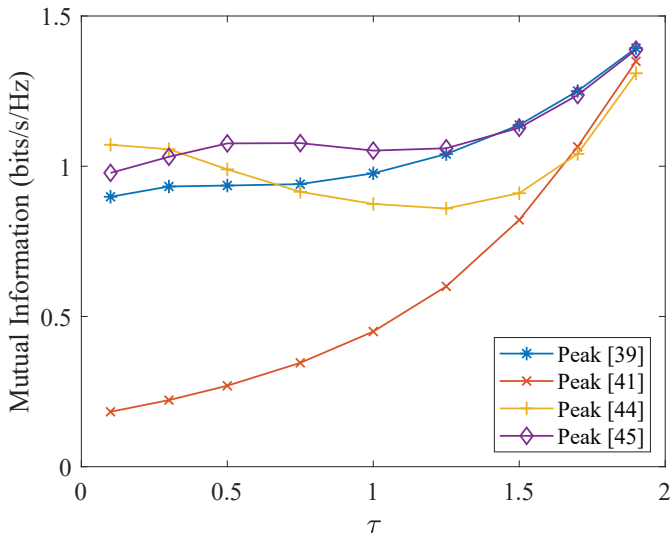
Fig. 15. System MI for the proposed algorithm with peak power limits using the heuristic EH model versus τ at $P_s = 20$dBm, $N = 2$.
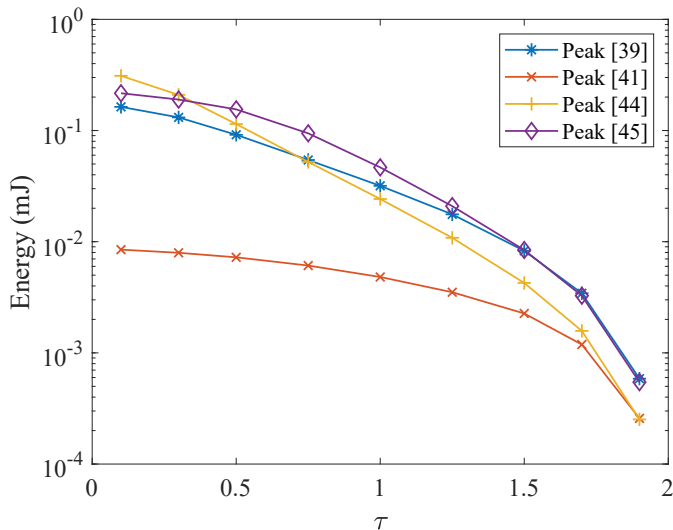

Fig. 16. Available Energy at the relay node for the proposed algorithm with peak power limits using the heuristic EH model versus τ at $P_s = 20$dBm, $N = 2$.

20dBm and $N = 2$, respectively, for different EH circuits. It is observed that the system MI for the proposed algorithm using the EH circuit [41] is the lowest compared to others. This is because the energy harvested by using the EH circuit [41] is the lowest as illustrated in Fig. 16. Furthermore, it is noted that the maximum energy efficiency for the EH circuit [41] ($\eta_{max} = 22\%$) is the lowest compared to the other considered EH circuits. Interestingly, it is observed that in most cases, when the EH relay node is implemented with practical EH circuit, the system MI increases with τ. This indicates that a better second-hop channel will help to improve the system MI.

V. CONCLUSION

In this paper, we have investigated the robust transceiver design for two-hop AF MIMO relay communication systems with the TSR protocol. The transceiver design with robustness assists in reducing the degradation caused by the CSI mismatch between the exact and estimated CSI available in the system. With the consideration of CSI mismatch, it can be seen that the optimization problem is more difficult to solve. We have used the KKT conditions with the primal decomposition method to solve the source and relay precoding matrices optimization problem. By using the golden section search method, we have obtained the optimized TS factor. It has been demonstrated through numerical simulations that the proposed transceiver design with robustness provides better performance compared to the non-robust transceiver design.

APPENDIX

From the problem (20), it is observed that $\mathbf{B}_e$ does not explicitly appear in the objective function (20a), however it influences (20a) by varying the feasible region of the problem (20) which is specified by constraints (20b) and (20c). According to *Lemma 2* in [46], it is noted that the optimal $\mathbf{B}_e$ is the one that maximizes the harvested energy at the relay during the first time frame. Hence, the optimal $\mathbf{B}_e$ is the solution to the problem given as

$$\max_{\mathbf{B}_e} E_h \left(tr \left\{ \mathbf{B}_e \mathbf{B}_e^H \mathbf{Q} \right\} \right) \tag{55a}$$

$$s.t. \ tr \left\{ \mathbf{B}_e \mathbf{B}_e^H \right\} = \lambda_e \tag{55b}$$

where λ_e is a positive scalar. As $E_h(x)$ in (3) is a non-decreasing function of x, it is noted that the problem (55) can be maximized by maximizing $tr \left\{ \mathbf{B}_e \mathbf{B}_e^H \mathbf{Q} \right\}$. Thus, the problem (55) is transformed into

$$\max_{\mathbf{B}_e} tr \left\{ \mathbf{B}_e \mathbf{B}_e^H \mathbf{Q} \right\} \tag{56a}$$

$$s.t. \ tr \left\{ \mathbf{B}_e \mathbf{B}_e^H \right\} = \lambda_e. \tag{56b}$$

The optimal structure of $\mathbf{B}_e$ is given as

$$\mathbf{B}_e = \mathbf{V}_q \mathbf{\Lambda}_e^{\frac{1}{2}} \mathbf{U}^H \tag{57}$$

where $\mathbf{\Lambda}_e$ is a diagonal matrix of size N_s and $\mathbf{U}$ is an $N_e \times N_s$ matrix satisfying $\mathbf{U}^H \mathbf{U} = \mathbf{I}_{N_s}$. The optimization problem (56) is expressed as

$$\max_{\tilde{\boldsymbol{\lambda}}_e} \sum_{i=1}^{N_s} \lambda_{q,i} \tilde{\lambda}_{e,i} \quad s.t. \sum_{i=1}^{N_s} \tilde{\lambda}_{e,i} = \lambda_e \tag{58}$$

where $\tilde{\boldsymbol{\lambda}}_e = [\tilde{\lambda}_{e,1}, \cdots, \tilde{\lambda}_{e,N_s}]^T$, $\lambda_{q,i}$ and $\lambda_{e,i}$ denote the ith diagonal elements of $\mathbf{\Lambda}_q$ and $\mathbf{\Lambda}_e$, respectively. Clearly, the optimal solution to the optimization problem (58) is $\tilde{\boldsymbol{\lambda}}_e^* = [\lambda_e, 0, \cdots, 0]^T$. By considering $\tilde{\boldsymbol{\lambda}}_e^*$, the optimal structure of $\mathbf{B}_e$ is rewritten from (57) into (21).

REFERENCES

[1] T. Huang, W. Yang, J. Wu, J. Ma, X. Zhang, and D. Zhang, "A Survey on Green 6G Network: Architecture and Technologies," *IEEE Access*, vol. 7, pp. 175758-175768, 2019.

[2] L. R. Varshney, "Transporting information and energy simultaneously," in *Proc. IEEE International Symposium on Information Theory*, Jul. 2008, pp. 1612-1616.

[3] X. Zhou, R. Zhang, and C. K. Ho, "Wireless information and power transfer: Architecture design and rate-energy tradeoff," *IEEE Transactions on Communications*, vol. 61, no. 11, pp. 4754-4767, Nov. 2013.

[4] R. Zhang and C. K. Ho, "MIMO broadcasting for simultaneous wireless information and power transfer," *IEEE Transactions on Wireless Communications*, vol. 12, no. 5, pp. 1989-2001, 2013.

[5] R. Jiang, K. Xiong, P. Fan, Y. Zhang, and Z. Zhong, "Power minimization in SWIPT networks with coexisting power-splitting and time-switching users under nonlinear EH model," *IEEE Internet of Things Journal*, vol. 6, no. 5, pp. 8853-8869, Oct. 2019.

[6] Y. Rong, "MIMO relay," in *Encyclopedia of Wireless Networks*, X. Shen, X. Lin, and K. Zhang, Eds. Cham: Springer International Publishing, 2018, pp. 1-4.

[7] A. A. Nasir, X. Zhou, S. Durrani, and R. A. Kennedy, "Relaying protocols for wireless energy harvesting and information processing," *IEEE Transactions on Wireless Communications*, vol. 12, no. 7, pp. 3622-3636, Jul. 2013.

[8] M. Maleki, A. M. D. Hoseini, and M. Masjedi, "Performance analysis of SWIPT relay systems over Nakagami-m fading channels with non-linear energy harvester and hybrid protocol," in *Proc. Iranian Conf. Electrical Engineering*, 2018, pp. 610-615.

[9] J. L. Bing, Y. Rong, L. Gopal, and C. W. R. Chiong, "Transceiver design for SWIPT MIMO relay systems with hybridized power-time splitting-based relaying protocol," *IEEE Access*, vol. 8, pp. 190922-190933, 2020.

[10] K. Xiong, P. Fan, C. Zhang, and K. B. Letaief, "Wireless information and energy transfer for two-hop nonregenerative MIMO-OFDM relay networks," *IEEE Journal on Selected Areas in Communications*, vol. 33, no. 8, pp. 1595-1611, Aug. 2015.

[11] B. Li and Y. Rong, "Joint transceiver optimization for wireless information and energy transfer in nonregenerative MIMO relay systems," *IEEE Transactions on Vehicular Technology*, vol. 67, no. 9, pp. 8348-8362, 2018.

[12] B. Li, M. Zhang, H. Cao, Y. Rong, and Z. Han, "Transceiver design for AF MIMO relay systems with a power splitting based energy harvesting relay node," *IEEE Transactions on Vehicular Technology*, vol. 69, no. 3, pp. 2376-2388, 2020.

[13] B. Li, H. Cao, Y. Rong, T. Su, G. Yang, and Z. He, "Transceiver optimization for DF MIMO relay systems with a wireless powered relay node," *IEEE Access*, vol. 7, pp. 56904-56919, 2019.

[14] Y. Rong, "Robust design for linear non-regenerative MIMO relays with imperfect channel state information," *IEEE Transactions on Signal Processing*, vol. 59, no. 5, pp. 2455-2460, May 2011.

[15] L. Gopal, Y. Rong, and Z. Zang, "Robust MMSE transceiver design for nonregenerative multicasting MIMO relay systems," *IEEE Transactions on Vehicular Technology*, vol. 66, no. 10, pp. 8979-8989, Oct. 2017.

[16] F. Benkhelifa and M. Alouini, "Precoding design of MIMO amplify-and-forward communication system with an energy harvesting relay and possibly imperfect CSI," *IEEE Access*, vol. 5, pp. 578-594, 2017.

[17] F. Benkhelifa, A. S. Salem, and M. Alouini, "Rate maximization in MIMO decode-and-forward communications with an EH relay and possibly imperfect CSI," *IEEE Transactions on Communications*, vol. 64, no. 11, pp. 4534-4549, 2016.

[18] R. Jiang, K. Xiong, P. Fan, L. Zhou, and Z. Zhong, "Outage probability and throughput of multirelay SWIPT-WPCN networks with nonlinear EH model and imperfect CSI," *IEEE Systems Journal*, vol. 14, no. 1, pp. 1206-1217, Mar. 2020.

[19] P. Shaik, P. K. Singya, N. Kumar, K. K. Garg, and V. Bhatia, "On impact of imperfect CSI over SWIPT device-to-device (D2D) MIMO relay systems," in *Proc. International Conference on Signal Processing and Communications (SPCOM)*, Bangalore, India, 2020, pp. 1-5.

[20] Q. Li and L. Yang, "Robust optimization for energy efficiency in MIMO two-way relay networks with SWIPT," *IEEE Systems Journal*, vol. 14, no. 1, pp. 196-207, Mar. 2020.

[21] H. Liu, K. J. Kim, K. S. Kwak, and H. Vincent Poor, "Power splitting-based SWIPT with decode-and-forward full-duplex relaying," *IEEE Transactions on Wireless Communications*, vol. 15, no. 11, pp. 7561-7577, Nov. 2016.

[22] J. Guo, S. Zhang, N. Zhao, and X. Wang, "Performance of SWIPT for full-duplex relay system with co-channel interference," *IEEE Transactions on Vehicular Technology*, vol. 69, no. 2, pp. 2311-2315, Feb. 2020.

[23] C. Zhong, H. A. Suraweera, G. Zheng, I. Krikidis, and Z. Zhang, "Wireless information and power transfer with full duplex relaying," *IEEE Transactions on Communications*, vol. 62, no. 10, pp. 3447-3461, Oct. 2014.

[24] P. N. Alevizos and A. Bletsas, "Sensitive and nonlinear far-field RF energy harvesting in wireless communications," *IEEE Trans. Wireless Commun.*, vol. 17, no. 6, pp. 3670-3685, June 2018.

[25] E. Boshkovska, D. W. K. Ng, N. Zlatanov, and R. Schober, "Practical non-linear energy harvesting model and resource allocation for SWIPT

systems," *IEEE Communications Letters*, vol. 19, no. 12, pp. 2082-2085, Dec. 2015.

[26] Y. Chen, K. T. Sabnis, and R. A. Abd-Alhameed, "New formula for conversion efficiency of RF EH and its wireless applications," *IEEE Transactions on Vehicular Technology*, vol. 65, no. 11, pp. 9410-9414, Nov. 2016.

[27] C. Xing, S. Ma, and Y. Wu, "Robust joint design of linear relay precoder and destination equalizer for dual-hop amplify-and-forward MIMO relay systems," *IEEE Transactions on Signal Processing*, vol. 58, no. 4, pp. 2273-2283, 2010.

[28] L. Musavian, M. R. Nakhai, M. Dohler, and A. H. Aghvami, "Effect of channel uncertainty on the mutual information of MIMO fading channels," *IEEE Transactions on Vehicular Technology*, vol. 56, no. 5, pp. 2798-2806, Sep. 2007.

[29] M. Ding and S. D. Blostein, "Maximum mutual information design for MIMO systems with imperfect channel knowledge," *IEEE Transactions on Information Theory*, vol. 56, no. 10, pp. 4793-4801, Oct. 2010.

[30] T. Yoo and A. Goldsmith, "Capacity and power allocation for fading MIMO channels with channel estimation error," *IEEE Transactions on Information Theory*, vol. 52, no. 5, pp. 2203-2214, May 2006.

[31] A. Antoniou and W.-S. Lu, *Practical Optimization: Algorithms and Engineering Applications*, 1st. Springer Publishing Company, Incorporated, 2007.

[32] J. L. Bing, L. Gopal, Y. Rong, C. W. R. Chiong, and Z. Zang, "Robust transceiver design for multihop AF MIMO relay multicasting from multiple sources," *IEEE Trans. Veh. Technol.*, vol. 70, pp. 1565-1576, Feb. 2021.

[33] D. P. Palomar and M. Chiang, "A tutorial on decomposition methods for network utility maximization," *IEEE Journal on Selected Areas in Communications*, vol. 24, no. 8, pp. 1439-1451, 2006.

[34] J. Hadamard, "Resolution d'une question relative aux determinants," *Bull. des Sciences Math.*, vol. 2, pp. 240-246, Sep. 1893.

[35] Y. Rong, X. Tang, and Y. Hua, "A unified framework for optimizing linear nonregenerative multicarrier MIMO relay communication systems," *IEEE Transactions on Signal Processing*, vol. 57, no. 12, pp. 4837-4851, Dec. 2009.

[36] Z. Fang, Y. Hua, and J. C. Koshy, "Joint source and relay optimization for a non-regenerative mimo relay," in *Proc. Fourth IEEE Workshop on Sensor Array and Multichannel Processing*, 2006, pp. 239- 243.

[37] I. Hammerstrom and A. Wittneben, "Power allocation schemes for amplify-and-forward MIMO-OFDM relay links," *IEEE Transactions on Wireless Communications*, vol. 6, no. 8, pp. 2798-2802, 2007.

[38] C. Song, J. Park, B. Clerckx, I. Lee, and K. Lee, "Generalized precoder designs based on weighted MMSE criterion for energy harvesting constrained MIMO and multi-user MIMO channels," *IEEE Transactions on Wireless Communications*, vol. 15, no. 12, pp. 7941-7954, 2016.

[39] T. Le, K. Mayaram, and T. Fiez, "Efficient far-field radio frequency energy harvesting for passively powered sensor networks," *IEEE J. Solid-State Circuits*, vol. 43, no. 5, pp. 1287–1302, May 2008.

[40] J. Guo and X. Zhu, "An improved analytical model for RF-DC conversion efficiency in microwave rectifiers," in *IEEE MTT-S Int. Microw. Symp. Dig.*, Jun. 2012, pp. 1–3.

[41] M. Stoopman, S. Keyrouz, H. J. Visser, K. Philips, and W. A. Serdijn, "A self-calibrating RF energy harvester generating 1V at -26.3 dBm," in *2013 Symposium on VLSI Circuits*, June 2013, pp. C226–C227

[42] E. Boshkovska, D. W. K. Ng, N. Zlatanov, A. Koelpin, and R. Schober, "Robust resource allocation for MIMO wireless powered communication networks based on a non-linear EH model," *IEEE Transactions on Communications*, vol. 65, no. 5, pp. 1984-1999, May 2017.

[43] R. Morsi, E. Boshkovska, E. Ramadan, D. W. K. Ng, and R. Schober, "On the performance of wireless powered communication with non-linear energy harvesting," in *2017 IEEE 18th International Workshop on Signal Processing Advances in Wireless Communications (SPAWC)*, 2017, pp. 1-5.

[44] J. Masuch, M. Delgado-Restituto, D. Milosevic, and P. Baltus, "An RF-to-DC energy harvester for co-integration in a low-power 2.4 GHz transceiver frontend," in *2012 IEEE International Symposium on Circuits and Systems (ISCAS)*, 2012, pp. 680-683.

[45] B. R. Franciscatto, V. Freitas, J. Duchamp, C. Defay, and T. P. Vuong, "High-efficiency rectifier circuit at 2.45 GHz for low-input-power RF energy harvesting," in *2013 European Microwave Conference*, 2013, pp. 507-510.

[46] F. Benkhelifa and M. Alouini, "Practical nonlinear energy harvesting model in MIMO DF relay system with channel uncertainty," in *2018 IEEE Global Communications Conference (GLOBECOM)*, 2018, pp. 1-7.

[47] K. Kotani, A. Sasaki, and T. Ito, "High-efficiency differential-drive CMOS rectifier for UHF RFIDs," *IEEE J. Solid-State Circuits*, vol. 44, no. 11, pp. 3011–3018, Nov. 2009.

Choo W.R. Chiong (Member, IEEE) received the B.E. (Hons.) and Ph.D. degrees in electrical engineering from Curtin University, Bentley, WA, Australia, in 2010 and 2015, respectively. He is currently a Senior Lecturer with the Department of Electrical and Computer Engineering, Curtin University, Malaysia Campus. His research interests include signal processing for communications and power system optimization.

Justin Lee Bing (Member, IEEE) received his Ph.D. degree in electronic and communication engineering from Curtin University, Bentley, WA, Australia, in 2021, and B.E. (Hons.) degree in electronic and communication engineering from Curtin University, Bentley, WA, Australia, in 2016. He is currently a device modeling engineer with the Custom Logic Engineering Programmable Solution Group (CLE-PSG), Intel Corporation, Penang, Malaysia. His research interests include machine learning, voice recognition, wireless communications, signal processing for communications, simultaneous wireless information and power transfer, and energy harvesting.
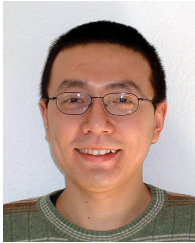
Yue Rong (Senior Member, IEEE) received the Ph.D. degree (*summa cum laude*) in electrical engineering from the Darmstadt University of Technology, Darmstadt, Germany, in 2005. He was a Post-Doctoral Researcher with the Department of Electrical Engineering, University of California, Riverside, from February 2006 to November 2007. Since December 2007, he has been with Curtin University, Bentley, Australia, where he is currently a Professor. His research interests include signal processing for communications, wireless communications, underwater acoustic communications, underwater optical wireless communications, applications of linear algebra and optimization methods, and statistical and array signal processing. He has published over 190 journal and conference papers in these areas.
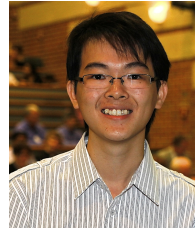
Dr. Rong was a recipient of the Best Paper Award at the 2011 International Conference on Wireless Communications and Signal Processing, the Best Paper Award at the 2010 Asia-Pacific Conference on Communications, and the Young Researcher of the Year Award of the Faculty of Science and Engineering at Curtin University in 2010. He is a Senior Area Editor of the IEEE Transactions on Signal Processing, and was an Associate Editor of the IEEE Transactions on Signal Processing from 2014 to 2018, an Editor of the IEEE Wireless Communications Letters from 2012 to 2014, and a Guest Editor of the IEEE Journal on Selected Areas in Communications special issue on theories and methods for advanced wireless relays. He was also a TPC Member for the IEEE ICC, IEEE GlobalSIP, EUSIPCO, IEEE ICCC, WCSP, IWCMC, and ChinaCom.

Lenin Gopal (Member, IEEE) received the B.Eng. degree in Electrical and Electronics Engineering from Madurai Kamaraj University, Madurai, India, in 1996, the M.Eng. degree in Telecommunications Engineering from Multimedia University, Cyberjaya, Malaysia, in 2006, and the Ph.D. degree from Curtin University, Bentley, WA, Australia, in 2015. He is currently an Associate Professor with the University of Southampton Malaysia (UoSM), Iskandar Puteri, Johor, Malaysia. His research interests include Signal Processing for Communications, Power Line Communications, and the Internet of Things (IoT).